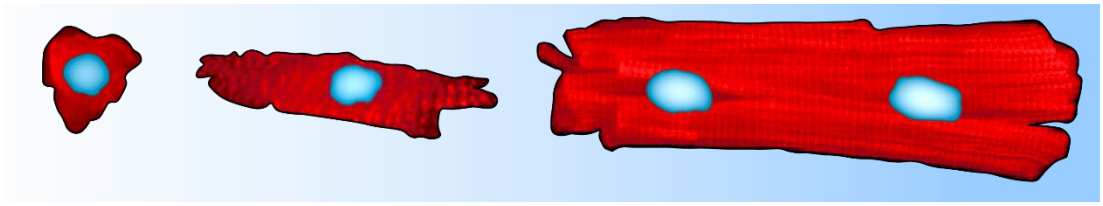

Restoring the heartbeat: Tracking cardiomyocyte proliferation

Rui Sérgio Ribeiro
Mestrado em Biologia Celular e Molecular
Departamento de Biologia
2015

Orientador
Tatiana Pinho Resende, Ph.D.
I3S - Instituto de Investigação e Inovação em Saúde
INEB – Instituto de Engenharia Biomédica

Coorientador
Perpétua Pinto-do-Ó, Ph.D.
I3S - Instituto de Investigação e Inovação em Saúde
INEB – Instituto de Engenharia Biomédica
ICBAS - Instituto de Ciências Biomédicas Abel Salazar

INSTITUTO DE INVESTIGAÇÃO E INOVAÇÃO EM SAÚDE
UNIVERSIDADE DO PORTO

INEB
Instituto de Engenharia Biomédica

U.PORTO
FACULDADE DE CIÊNCIAS
UNIVERSIDADE DO PORTO

Todas as correções determinadas pelo júri, e só essas, foram efetuadas.

O Presidente do Júri,

Porto, _____/_____/_____

This Thesis was performed under the supervision of:

Supervisor:

Tatiana P. Resende, Ph.D. - I3S - Instituto de Investigação e Inovação em Saúde, Universidade do Porto, Portugal; INEB - Instituto de Engenharia Biomédica, Porto, Portugal.

Co-supervisor:

Perpétua Pinto-do-Ó, Ph.D. - I3S - Instituto de Investigação e Inovação em Saúde; INEB - Instituto de Engenharia Biomédica; Instituto de Ciências Biomédicas Abel Salazar (ICBAS), Universidade do Porto, Porto, Portugal.

The work presented in this Thesis was performed in the following institution:

I3S - Instituto de Investigação e Inovação em Saúde, Universidade do Porto, Portugal.
INEB - Instituto de Engenharia Biomédica, Rua do Campo Alegre 823, 4150-180, Porto, Portugal.

Funding:

This work was funded by PTDC/SAU-ORG/118297/2010 and performed in the framework of the projects PEst-C/SAU/LA0002/2011 and Pest-C/SAL/LA0002/2013 from the Portuguese Foundation for Science and Technology (FCT), Quadro de Referência Estratégico Nacional (QREN), Fundo Europeu de Desenvolvimento Regional (FEDER) and Programa Operacional Regional do Norte (ON.2-O Novo Norte) [NORTE-07-0124-FEDER-000005-Project on Biomedical Engineering for Regenerative Therapies and Cancer; "ACTION2"].

AGRADECIMENTOS

À minha orientadora, Tatiana Resende, um grande obrigado por tudo o que me ensinaste, por toda a dedicação, preocupação e amizade ao longo desta "epopeia" bem-sucedida!

Um muito obrigado à Doutora Perpétua Pinto-do-Ó, pela oportunidade de integrar o seu fantástico grupo de investigação, por todo o apoio mesmo perante uma "agenda apertadíssima" e por me ter dado a conhecer um pouco deste vasto mundo da Biologia do Desenvolvimento.

À restante *Heart Team* - Diana, Ana Freire, Mariana, Ana Silva, Tiago L., Vasco, Francisca e Sílvia – que mais do que um grupo de investigação, se tornou uma segunda família, sempre com grande disponibilidade e muitos momentos hilariantes.

À Pipa (*por tudo! lógico né!*), Bia (*a rainha suprema!!!*), Rúben (*e seu semblante sempre "sério"*), Dani Salvador (*sempre podendo, aqui ou no UK!*), Rubi (*palavras para quê?!*), Rita Bento (*e os seu mil mistérios!*), Dani Barros (*a "vizinha" dos milhentos géis e proteínas!*), Sara (😜), Ritinha, Estrelinha, Graciosa, Cati e João V., entre muitos outros….. E mais uma vez, Tiago (*graças a ti agora sim domino fórmulas de Excel, "sopas" e "aspiradores"*), Ana Freire (*slay those NY b****es! e que nunca faltem as sandes de presunto à minha eterna manager!*), Aninhas ("*you woke up flawless!"*), Vasco (*meu companheiro alfacinha de immunos, obrigado por toda a ajuda, pelos cafés, conversas e boleias*), Sílvia (*obrigado por toda a ajuda, rimo-nos muito naquele piso -1 e no meio de tanta immuno!*) e Francisca (*obrigado pela tua boa-disposição sempre contagiante*). A todos, obrigado por me deixarem fazer parte da "família INEBiana", pela amizade, cumplicidade, paciência, companheirismo, generosidade, loucura e todas as *happy hours* e *chill-outs*!

Aos meus "#MigosLokitos" super turbinadíssimos - Andreia, Sílvia, Steeve, Patrícia e Ana - um grande obrigado por tudo o que partilhámos ao longo destes 5 anos de faculdade!

E aos meus pais, por todo o apoio incondicional.

"Cada amigo novo que ganhamos no decorrer da vida aperfeiçoa-nos e enriquece-nos, não tanto pelo que nos dá, mas pelo que nos revela de nós mesmos!"

(Miguel de Unamuno y Jugo, "O Segredo da Vida")

ABSTRACT

The heart is the first organ to become fully functional in the vertebrate embryo. Cardiomyocytes (CMs) are the major structural constituents of the heart and are severely affected in a heart failure situation. Through embryogenesis, mononucleated diploid CMs intensively proliferate but shortly after birth undergo terminal differentiation, which comprises sarcomere assembly and a drastic morphological rearrangement, from round to rod shape. This correlates with CMs' cytokinesis blockage and cell cycle withdrawal, culminating in binucleation or polyploidy (according to the species) and cessation of proliferation. Subsequently, cardiac growth results from cell hypertrophy. While the mammalian heart has been considered a post-mitotic organ, devoid of intrinsic proliferative capacity, recent reports on CMs renewal in the adult murine and human hearts have challenged this longstanding dogma. However, the cellular renewal's magnitude remains elusive due to tissue complexity, hurdles in isolating adult CMs and unavailability of specific CMs surface markers. Even though important advances have been made in recent years, distinct aspects of CMs maturation and differentiation remain elusive. For example, no data is available when considering the relationship between CMs' morphometry and proliferation ability along ontogeny. Likewise, CMs' cell cycle progression and/or duration remains poorly comprehended.

This study set out to perform a detailed characterization of the CMs' morphometry, nuclear and cell cycle dynamics, along mouse ontogeny. By combining a novel CMs isolation protocol with imaging flow cytometry we were able to successfully obtain a high yield of well-preserved CMs and collect quantitative data and imagery, enabling multiparametric analysis of CMs. Using ImageStream^X we demonstrated that at around embryonic day E17.5, CMs undergo elongation and multinucleation, resulting in rod-shaped cells with up to four nuclei at P10. Concerning the cell cycle and proliferation dynamics, our data demonstrate a gradual decrease of the cell cycle activity and mitotic CMs within the murine heart, as it matures along ontogeny. Finally, we have identified a stable and small fraction of immature mononucleated and round-shaped cells in the late developmental stages, which might putatively maintain mitosis-competence, being thus of potential therapeutic interest and the starting point for further studies.

Keywords: cardiomyocytes, cell cycle status, heart, ImageStream^X, maturation, mitosis, ontogeny, proliferation.

RESUMO

O coração é o primeiro órgão a tornar-se completamente funcional nos vertebrados. Os cardiomiócitos (CMs) são o principal constituinte estrutural do coração, sendo severamente afetados num cenário de doença cardiovascular. Durante a embriogénese dos mamíferos, CMs mononucleados e diplóides proliferam intensivamente, mas após o nascimento sofrem diferenciação terminal com maturação dos sarcómeros e rearranjo da morfologia da célula, que passa de circular para retangular. Este evento está correlacionado com um bloqueio da citocinese e consequente saída do ciclo celular, culminando em binucleação ou poliploidia (consoante a espécie) e no cessar da sua capacidade proliferativa. Consequentemente, o crescimento do coração resulta da hipertrofia dos CMs. O coração do mamífero adulto tem sido considerado um órgão pós-mitótico, desprovido de capacidade proliferativa. Contudo, relatos recentes de renovação celular nos corações de ratinho e humano adulto vieram contradizer este dogma. No entanto, a magnitude desta renovação celular permanece incerta, o que se deve à complexidade celular do coração, às dificuldades em isolar CMs adultos e à ausência de marcadores de superfície específicos para estas células. Apesar de nos últimos anos terem surgido novos dados sobre a maturação dos CMs, diferentes aspetos da sua biologia permanecem por esclarecer. Nomeadamente, não existem dados sobre a relação entre a morfologia dos CMs e a sua capacidade proliferativa. Para além disso, a progressão dos CMs no ciclo celular e a sua duração permanecem pouco caracterizadas.

O presente estudo teve como objetivo realizar uma caracterização da dinâmica da morfometria, número de núcleos e ciclo celular dos CMs ao longo da ontogenia de murganho. Combinando um protocolo de isolamento novo com uma técnica de citometria de fluxo com imagem, conseguimos obter uma boa amostragem de CMs com estrutura preservada e recolher dados quantitativos das células. Usando o ImageStream^X demostrámos que, por volta do dia embrionário E17.5, os CMs sofrem elongação e multinucleação, resultando em células com forma de bastonete e que podem ter até quatro núcleos no dia pós-natal 10. Relativamente à dinâmica do ciclo celular e proliferação, os dados apontam para um decréscimo gradual do número de células ativas e mitóticas, à medida que o coração matura. Finalmente, foi também identificada uma pequena e estável fração de células imaturas, mononucleadas e redondas, nas fases finais da ontogenia, que poderão permanecer mitoticamente ativas, despertando assim interesse terapêutico e motivando o início de diversos estudos.

Palavras-chave: cardiomiócitos, ciclo celular, coração, ImageStream^{X}, maturação, ontogenia, proliferação.

TABLE OF CONTENTS

LIST OF TABLES AND FIGURES

LIST OF ABBREVIATIONS

- ANOVA Analysis of variance
- AR Aspect ratio
- BSA Bovine serum albumin
- CDKs Cyclin-dependent kinases
- CMs Cardiomyocytes
- CVDs Cardiovascular diseases
- Cnx Connexin
- DAPI 4',6-diamidino-2-phenylindole
- DNA Deoxyribonucleic acid
- E Embryonic day
- ESCs Embryonic stem cells
- EMT Epithelial-mesenchymal transition
- FBS Fetal bovine serum
- FHF First heart field
- HBSS Hank's Balanced Salt Solution
- ICC Immunocytochemistry
- ICD Intercalated discs
- Ig Immunoglobulin
- IHC Immunohistochemistry
- iPSCs Induced pluripotent stem cells
- M Molar
- MHC Myosin heavy chain
- MI Myocardial infarction
- min Minutes
- mL Milliliter
- OFT Outflow tract
- ON Overnight
- P Postnatal day
- PB Phosphate buffer
- PBS Phosphate-buffered saline
- PE Proepicardium
- PFA Paraformaldehyde

- pH3 Phosphorylated Histone H3
- PS Primitive streak
- RT Room temperature
- SD Standard deviation
- SHF Second heart field
- WHO World Health Organization
- µm Micrometers
- µM Micromolar

INTRODUCTION

The adult heart: an overview

The heart is a muscular organ, which synchronous contractions are responsible for supporting blood passage through the circulatory system, providing oxygen and nutrients, as well as removing metabolic wastes. Anatomically, the mammalian heart comprises four chambers which support a double-circulation system: two blood-receiving atria and two blood-pumping ventricles (Fig.1A). The right atrium receives venous blood from the whole body, through the venae cavae, passes it to the right ventricle, through the tricuspid valve, which pumps it into the pulmonary artery to the lungs. Oxygenated blood from the lungs, returns to the left atrium, via pulmonary arteries, and flows to the left ventricle (passing through the mitral/bicuspid valve), then being pumped into the aorta, to enter the whole-body systemic circulation (Lin et al., 2012). At the cellular level, the heart displays an astonishing complexity, comprising CMs, fibroblasts, hematopoietic and endothelial cells, vascular smooth muscle cells and specialized cells of the conduction system (Fig.1B). Conjointly these cells dynamically contribute to the structural, mechanical, chemical and electrical properties of an efficient heart, communicating with each other via autocrine, paracrine and cell-cell interactions (Harvey & Rosenthal, 1999). The heart wall exhibits a three-layered composition, encompassing the inner endocardium, a layer of endothelial cells lining the cardiac chambers and covering the heart valves; the myocardium, which is the thickest layer, composed of contractile cardiac muscle cells (cardiomyocytes – CMs); and the outer epicardium, constituted by epithelial cells. This is also the innermost layer of the pericardium, a double-walled sac which encloses the heart in the thoracic cavity (Fig.1).

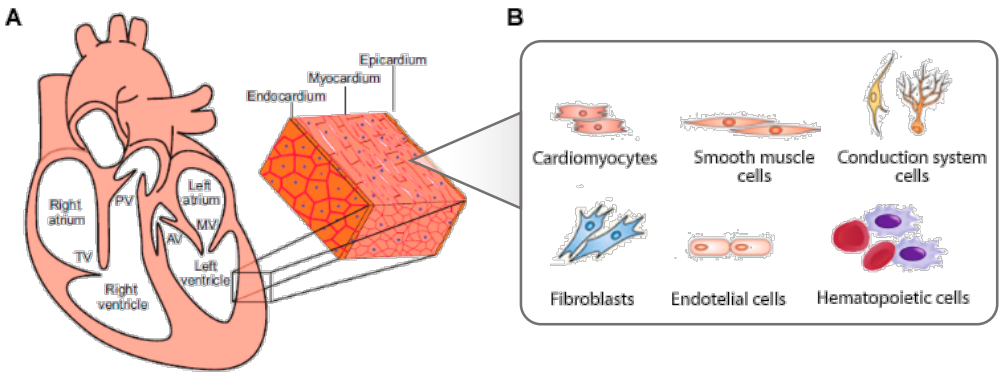

Fig.1 - The adult mammalian heart and its cellular complexity. A mature mammalian heart contains two atria, two ventricles and four valves determining the blood flow. The wall of each chamber consists of three tissue layers: endocardium, myocardium and epicardium. The main cellular components of the mature mammalian heart are contractile

cardiomyocytes, endothelial and hematopoietic cells, fibroblasts, smooth muscle vascular cells and specialized conduction system cells. Adapted from Xin et al. (2013).

Cardiovascular diseases (CVDs) are the top cause of morbidity and mortality in the western world. World Health Organization (WHO) reported an estimated 17.3 million victims from CVDs in 2008, and by 2030 more than 23 million people are predicted to die annually from these disorders (WHO, 2010; WHO, 2011).

Myocardial infarction (MI), or heart failure, is the most common cardiac disorder, and it is caused by occlusion of a coronary artery due to a blood clot or an atherosclerotic plaque, leading to myocardial ischemia and subsequent necrosis. Along with massive CMs death, the necrotic tissue is gradually replaced by a collagen scar, unable of contractile movements, diminishing the cardiac output and favoring the emergence of progressive compensatory pathologies (e.g. ventricular chamber dilation with wall thinning, arrhythmias, cardiogenic shock or a second MI) (Laflamme & Murry, 2005). Apart from heart transplantation and ventricular assist devices (electromechanical circulatory device used to partially or completely replace the function of a failing heart - Website 1), present-day therapies (thrombolytic drugs administration, bypass surgery or percutaneous coronary intervention), do not address the critical problem of a diminished pumping capacity, owing to a reduced pool of contractile muscle cells. Thus, for several years the focus of regenerative medicine has been on finding endogenous or external sources of cells to repopulate the injured area and stimulate intrinsic proliferation. These endogenous cells types, identified in mice and human, include the c-Kit (Beltrami et al., 2003), Isl1 (Cai et al., 2003) and Sca1-positive (Matsuura et al., 2004) resident cardiac progenitors, side-population cells which are able to efflux Hoechst DNA dye (Pfister et al., 2005) and cardiospheres-derived stem cells (Messina et al., 2004). Exogenously delivered cell-based therapies using human embryonic stem cells (ESCs) or induced pluripotent stem cells (iPSCs) have also been proposed to repopulate the injured area and stimulate intrinsic proliferation (Laflamme et al., 2007; Matsuura et al., 2012). Some of these cells have even been used in clinical trials: ALCADIA (Takehara et al., 2008) and CADUCEUS (Makkar et al., 2012) used cardiospheres-derived stem cells, whereas SCIPIO (Bolli et al., 2011) used c-Kit-expressing cells. The efficiency of these approaches remains modest with two major concerns arising from their use: the patients' safety during and after cell deliver, and tracking the cells to their ultimate destination, as diffusion to the blood circulation may occur, which can cause side-effects (Goldthwaite Jr, 2007). Low cell retention and engraftment in the healthy myocardium, low efficiency of cardiogenic differentiation and teratoma formation have also been hampering the

success of these regenerative therapies (Malliaras & Marban, 2011). Alternatively, the administration of exogenous growth factors or cytokines to stimulate uninjured cardiomyogenic progenitors or preexistent CMs adjacent to the injured area, is also under investigation (Kuhn et al., 2007). The adult mammalian heart has been considered as a post-mitotic organ due to its limited regenerative capacity. This contrasts with animal models such as zebrafish, which is capable of fully regenerating the heart after surgical resection of up to 20% of the ventricular region (Poss et al., 2002). This has been correlated with the proliferative capacity of CMs (Wills et al., 2008) and little inflammatory response after cardiac injury (Ieda et al., 2009). The longstanding dogma of the adult mammalian heart being devoid of intrinsic proliferation, has been however challenged by different observations. In 1998, Kajstura et al. (1998) demonstrated by immunocytochemistry a mitotic index of 14 proliferating CMs per million of myocytes in human diseased hearts (Kajstura et al., 1998). Ten years later, the radiocarbon-based tracing study of Bergmann et al. (2009) shown a CMs turnover' rate of 1% per year at the age of 25, decreasing to 0.45% at the age of 75 (Bergmann et al., 2009). Recently, other reports of human CMs renewal arose, such as the one from Kajstura et al. (2010), in which the fraction of adult human CMs labeled by iododeoxyuridine ranged from 2.5% to 46%, and the one from Mollova et al. (2013), which demonstrated by immunofluorescence on myocardial samples-derived CMs, an extent of mitosis of ~0.04% at birth and ~0.009% between the second decade of life (Kajstura et al., 2010; Mollova et al., 2013). After myocardial infarction, adult murine hearts also display a low extent of CMs replenishment ability (23% of CMs showed ^{15}N-nuclear labelling, in contrast with 4.4% in unoperated mice, in Senyo et al. (2013) work). The observed proliferation is albeit insufficient to repair extensive injuries (Senyo et al., 2013).

Remarkable CMs regenerative capacity has also been demonstrated during murine embryonic development (Drenckhahn et al., 2008) and in the early postnatal period upon cardiac injury (Porrello et al., 2011). However, the magnitude at which CMs renewal occurs is still under debate. In fact, the exact number of CMs within the murine adult heart remain uncertain, accounting from 15-56% of the total number of cardiac cells, based on histology and flow cytometry data (Nag, 1980; Vliegen et al., 1991; Banerjee et al., 2007). The inconsistencies in mammalian adult CMs' proliferation rates reported in the literature (ranging from less than 1% to more than 40% per year) (Soonpaa & Field, 1997; Kajstura et al., 2010), are mainly due to difficulties in isolating and accurately identifying these cells within the cardiac tissue due to its inherent complexity and to the absence of specific cardiomyocytic surface markers. Current identification of CMs is mostly based on immunolabelling of components of the

sarcomeric apparatus (e.g. cardiac troponin T and I, sarcomeric α-actinin and α-actin). Therefore, decoding the mechanisms underlying the embryonic heart development and CMs' maturation emerges as a crucial step to identify a specific marker and gain deeper insight into CMs' biology.

Mammalian cardiogenesis: an overview

The heart is the first functional organ formed during embryonic development, due to its vital role in blood and nutrients supply (Lyons, 1996). Its formation is a complex morphogenic event dependent of coordinated contribution of cardiac progenitor cells, derived from three precursors pools spatiotemporally segregated in the developing embryo: cardiogenic mesoderm, cardiac neural crest and the proepicardium (Vincent & Buckingham, 2010). Cardiogenesis starts with the formation of the cardiogenic mesoderm during embryo gastrulation (murine embryonic day [E] 6.5) (Fig.2) - a key event where the three germ layers (endoderm, mesoderm and ectoderm) are formed, by ingression of the epiblast cells through the primitive streak (PS) (Tam et al., 1997). Cardiac mesodermal progenitor cells are then instructed to adopt a cardiac fate, forming two subpopulations. The path followed by these mesodermal progenitors to achieve full differentiation is rigorously controlled and regulated by numerous transcriptional cardiac regulators and signaling pathways, such as Wnt, Nodal and Notch (Freire & Resende, 2014). The earliest subset, known as first heart field (FHF) migrates from the splanchnic mesoderm to an anterior-lateral position relative to the PS, and under the head folds, forming two bilaterally symmetrical cardiac regions. Once shaped, it expands and coalesce establishing the cardiac crescent. Lying underneath this structure emerges the second heart field (SHF), derived from the pharyngeal mesoderm (E7.5 - Fig.2) (Buckingham et al., 2005; Tzahor & Evans, 2011). The horseshoe-shaped cardiac crescent then suffers midline fusion forming the primitive cardiac tube (E8 - Fig.2), consisting of an outer layer of CMs (primitive myocardium) and an inner layer of endothelial cells (primitive endocardium). The first contractions occur at this stage, starting as peristaltic movements that progress into rhythmic contractions (Moorman & Christoffels, 2003). The heart tube rapidly expands through the recruitment of proliferating cells from the heart fields. While FHF contributes to the primitives left ventricle and atria, the SHF supports the primitive right ventricle and the outflow tract, a temporary embryonic structure that connects the ventricles with the aortic sac, ultimately generating the base of the ascending aorta and the pulmonary trunk.

At E8.5 rightward-looping occurs with the posterior region of the tube moving anteriorly to position the cardiac chambers for proper development (Fig.2) (Tzahor & Evans, 2011). Other cellular populations, such as the proepicardium and the cardiac neural crest, contribute at this stage to heart formation. The proepicardium (PE) is a transitory cell cluster that arises near the venous pole of the heart tube (E8.5). PE-derived cells enclose the naked myocardium, forming the epicardium layer (E9.5-E11.5) (Cai et al., 2008), and some invade the heart experiencing epithelial-mesenchymal transition (EMT) [a biological process by which epithelial cells lose their cell polarity and cell-cell adhesions, assuming a mesenchymal phenotype with enhanced migratory and invasive properties, high resistance to apoptosis and absence of polarity, allowing their differentiation into a multiplicity of cell types (Kalluri & Weinberg, 2009)]. These cells differentiate into cardiac fibroblasts, coronary vessels' smooth muscle and, and to a less extent into CMs and endothelial cells (Manner et al., 2001; Vincent & Buckingham, 2010). Recently, cell clusters with canonical stem-features (e.g. fibronectin encasement, vascular support) were described to be dispersed along the epicardial layer and suggested to have a role in the limited regenerative capacity of the adult heart in a cardiovascular disease setting (Balmer et al., 2014). Cardiac neural crest cells are a temporary subpopulation of cranial neural crest-derived cells, emergent from the dorsal neural tube (Kirby, 1987). These pluripotent cells actively migrate towards the heart at E10.5, guided by chemotactic routes after undergoing EMT, contributing for the aortic arteries development, myocardium septation, valve formation and for cardiac autonomic nervous system (Kuriyama & Mayor, 2008; Jain et al., 2011).

By E14.5, the cardiac chambers are formed and the heart undergoes maturation. This comprises atria and ventricles' septation, formation of the atrioventricular junction and the development of the atrioventricular cushions that will later give rise to the tricuspid and mitral valves (Marín-García, 2011). In the end, the heart achieves its final shape with a three-layered wall and fully-septated and well-defined cardiac chambers, connected to the pulmonary trunk and aorta.

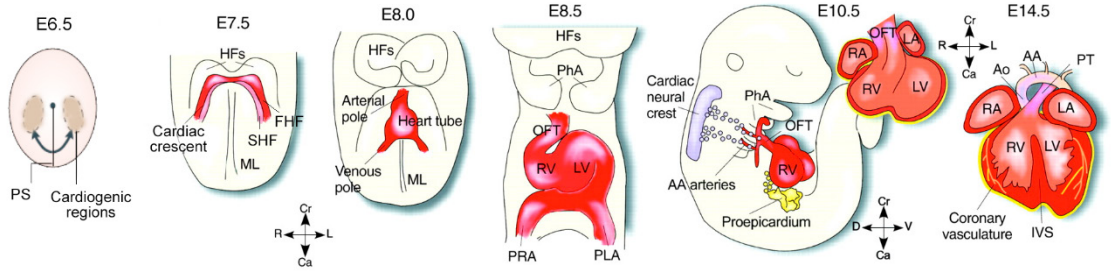

Fig.2 - Developmental stages of mammalian cardiogenesis. Myocardial progenitor cells ingress through the primitive streak (PS), migrating to the anterior of the embryo at about embryonic day (E) 6.5. These cells come to lie under the head folds (HFs), on each side of the PS, forming the first heart field (FHF) that will coalesce, resulting in the cardiac

crescent, where differentiated myocardial cells are now observed (E7.5). Underneath the cardiac crescent lies the second heart field (SHF), originated from the pharyngeal mesoderm. Next, the cardiac crescent expands, through recruitment of cells from FHF and SHF, fusing at the midline (ML) and forming the early beating heart tube (E8). Rightward-looping occurs (E8.5), resulting in the establishment of primitive ventricles and atria. After the looping, cardiac neural crest and proepicardium-derived cells contribute to the outflow tract (OFT) and epicardium development, respectively. By E10.5, the heart has acquired well-defined chambers, which by E14.5 become totally individualized by septation, and connected to the pulmonary trunk (PT) and aorta (Ao). IVS, interventricular septum; LA, left atrium; LV, left ventricle; PhA, pharyngeal arches; PLA, primitive left atrium; PRA, primitive right atrium; RA, right atrium; RV, right ventricle. Cranial (Cr)-caudal (Ca), right(R)-left (L) and dorsal (D)-ventral (V) axes are indicated. Adapted from Laugwitz et al. (2008).

Ventricular wall: Trabeculation & Compaction

Throughout cardiogenesis, myocardium layer displays polarized growth, resultant from oriented and exponential CMs division (Meilhac et al., 2004). At the heart-tube stage (E8 - Fig.3), the ventricular wall is composed by one or two cells-thick layer of contractile myocardium, a single-cell layer of endocardium and, sandwiched in between, cardiac jelly - an acellular gelatinous matrix secreted by the myocardium (Bartman & Hove, 2005). As the heart tube undergoes rightward-looping, the ventricular myocardium thickens and the endocardial and inner myocardial layers invaginate (E9.5-E10.5 - Fig.3), forming myocardial trabeculae projected into the lumen and supported by a basal layer of compact myocardium (Zhang et al., 2013). The development of ventricular trabeculae is governed by signal transduction pathways involving the endocardium, myocardium and cardiac jelly. Trabeculae rapidly elongate, enhancing the contractile CMs' force and the diffusion of oxygen and nutrients to the developing heart (E12.5-E13.5 - Fig.3) (Sedmera et al., 2000). Trabeculae expansion is achieved through proliferation of CMs, being that the proliferative capacity of the compact layer is significantly higher than that of the trabecular layer, exhibiting a 2-fold greater rate of cell division (Walsh, 2005). A transmural cell cycle gradient of decreasing proliferation and increasing differentiation of CMs is thus formed towards the apex of the trabeculae (Meilhac et al., 2003; de Boer et al., 2012). Around E14.5, the compact layer is highly proliferative and the trabeculae start to compact at their base, resulting in a compact and dense ventricular wall (Fig.3). From E16 onwards, the compact layer proliferates and matures into a complex and multilayered structure, and as a consequence of the increased contractile force required for systemic circulation, the compact layer of the left ventricle grows thicker than that of the right ventricle, in the adult mammalian heart (Risebro & Riley, 2006; Zhang et al., 2013).

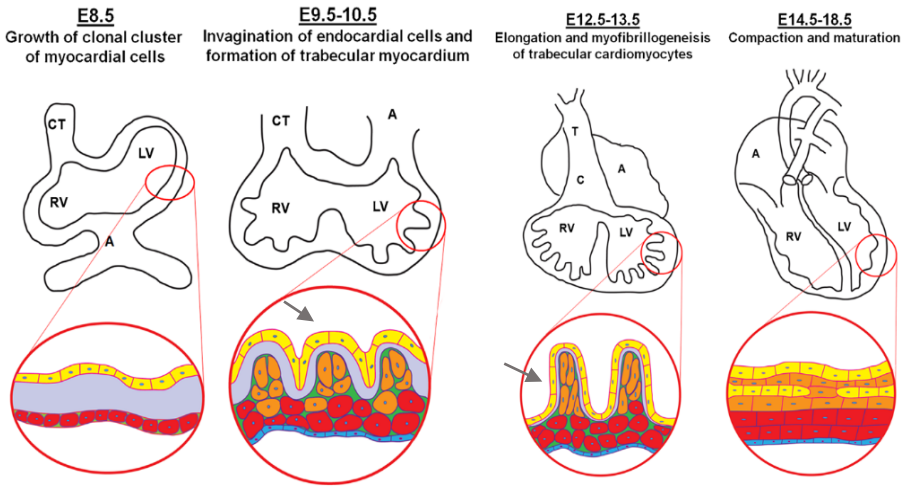

Fig.3 - Development of the ventricular wall. At E8.5, the cardiac tube is comprised by a thin layer of myocardium (red), separated by acellular cardiac jelly (grey) from the endocardium (grey). As it undergoes rightward-looping during E9.5-E10.5, prominent trabeculae (grey arrows) emerge supported by a thin layer of proliferative compact myocardium. Elongation of trabeculae occurs during E12.5-E13.5. By E14.5 compaction occurs, contributing to the thickening and maturation of the ventricular wall, which is already covered by the epicardium (blue). Adapted from Zhang et al. (2013).

Cardiomyocytes: Maturation and Differentiation

Cardiomyocytes exhibit highly specialized components crucial for their proper function, i.e. to generate coordinated contractions for proper blood circulation: (1) sarcomeres, which are repetitive subunits of actin and myosin filaments tightly stacked, composing the basic mechanical unit to produce contractile force; and (2) intercalated discs (ICD), located at the cells' apical ends, consisting of desmosomes, adherens junctions and gap junctions, that together mediate electro-mechanical coupling and intercellular communication (Sarantitis et al., 2012).

Mammalian cells' proliferation and differentiation are closely related to each other, and are regulated in an inverse fashion (Studzinski & Harrison, 1999). Myocardial growth occurs in two temporally distinct phases. During embryogenesis, heart growth occurs by hyperplasia, in which mononucleated diploid CMs with immature sarcomeres intensely proliferate (Oparil et al., 1984). Disassembly of the sarcomeric apparatus is crucial for proliferation, however the mechanisms responsible for sarcomere collapse and their *de novo* formation are not totally comprehended (Kaneko et al., 1984; Ahuja et al., 2004). In the first two weeks following birth, major alterations occur in CMs and after the fifth postnatal day (P5) (Leu et al., 2001), cardiac growth occurs essentially by CMs hypertrophy (around 30-40 fold cell volume increase) (Oparil, 1985). In mammals, this neonatal transition is linked with terminal differentiation and according to the species, it

is accompanied by CMs binucleation (mouse) or polyploidization (human), both correlating with the onset of CMs cell cycle withdrawal to a quiescent G0 phase. In mice, this neonatal transition is marked by extensive CMs binucleation between P5-P10 resulting from a final round of acytokinetic mitosis, with up to 90% of adult murine CMs becoming binucleated during the first two postnatal weeks (P0-P14) (Soonpaa et al., 1996; Soonpaa & Field, 1997). In contrast, by the onset of puberty most of human CMs are mononucleated and polyploid, with ploidy as high as 64N (Laflamme & Murry, 2011; Mollova et al., 2013). A considerable fraction (25%) of binucleated diploid (2x2N) cells is also reported to exist in the adult heart (Olivetti et al., 1996; Steinhauser & Lee, 2011).

With terminal differentiation, CMs cellular dimensions and shape are also drastically restructured. Hirschy et al. (2006) characterized CMs' transformation along maturation: longitudinal growth results from increased myofibrils' length and number, their tight stacking and re-orientation into a parallel orientation (Fig.4). This drastic reorganization of the cell cytoarchitecture is accompanied with ICD formation and redistribution. ICD present a circumferential pattern in early embryonic CMs and is restricted to the cell's apical ends by birth (Fig.4) (Perriard et al., 2003; Hirschy et al., 2006). Major alterations are also detected in the expression of contractile proteins-coding genes, such as replacement of α-skeletal actin and β-MHC in the murine fetal heart by α-cardiac actin and α-MHC. As a result of these modifications, the sarcomeric apparatus becomes denser and more complex in the early neonatal stages, providing a better adaptation to the after-birth systolic load intensification (Ng et al., 1991; Driesen et al., 2009). Simultaneously, the expression pattern of the connexin (Cnx) protein family (present in gap junctions) changes: Cnx-40 and -45 predominate in embryonic CMs, being later replaced at E18.5 by the isoform Cnx-43 (Delorme et al., 1997; Hirschy et al., 2006). The switch in the cardiac genetic profile is also complexly linked with the remodeling of the epigenetic context. Embryonic CMs display histone modifications for active genetic expression of proliferation-related genes, such as hyperacetilation (H3K9/14ac, H3K18ac, and H3K27ac) and phosphorylation of histone H3 (H3S10ph, considered a hallmark of mitosis). Extensive chromatin condensation (heterochromatin) resultant from its deacetilation (at H3K9/14, H3K18, and H3K27) and methylation (H3K9me2/3 and H3K27me3) is observed throughout CMs terminal differentiation, culminating in transcriptional repression of embryonic cardiac genes and upregulation of adult cardiac-specific genes together with the silencing of cell cycle genes (Sdek et al., 2011; Oyama et al., 2014).

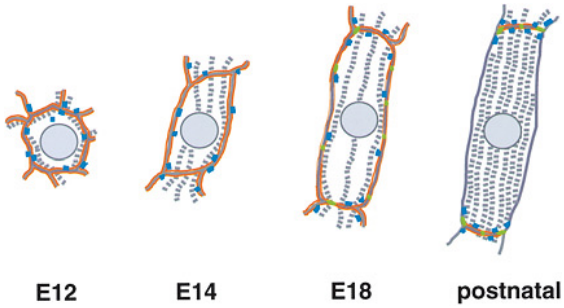

Fig.4 - Schematic representation of the changes in cellular shape, myofibril alignment and cell-cell contact organization that take place in CMs during mouse heart development. The early embryonic CMs (E12) have a round shape, few myofibrils (grey), and adherens junctions (orange) and desmosomes (blue) homogenously distributed. Around E14, CMs elongation initiates with myofibrillar alignment, but the cell–cell contacts are still broadly distributed. By E18, the adherens junctions begin to be restricted to the apical ends of the CMs, where the myofibrils are inserted, and the gap junctions (green) are still located in the lateral surface. The final arrangement of the intercalated discs is achieved only after birth, with the cell-cell contacts being totally restricted to the polar ends. Reproduced from Perriard et al. (2003).

Cell cycle withdrawal: a multifactorial event

The typical mammalian cell cycle, by which cells divide, is composed of interphase (G1, S and G2 phases) and M-phase (mitosis), which culminates with karyokinesis and cytokinesis. Cell cycle progression entails a tightly regulation by cyclins and their targets, the cyclin-dependent kinases (CDKs). In mammals, cyclins-CDKs complexes are sequentially formed and regulated to orchestrate coordinated entry into the next phase of the cell cycle. Cytokinesis is the final step of mitosis culminating in the physical division of the two daughter cells, with proper inheritance of both nuclear and cytoplasmic contents. This cell cycle phase consists of a chain of events involving: (1) the establishment of the division plane; (2) furrow ingression by the actinomyosin contractile ring, which position in the cell's cortex is defined by distinct proteins, such as anillin; (3) formation of the midbody, a transitory cytoskeletal structure that localizes the site of abscission; and finally (4) cell separation in a process called abscission (Field & Alberts, 1995; Glotzer, 2001).

Several studies have focused on the genetic and molecular changes associated with CMs cell cycle arrest, but the multifactorial network governing this event remains largely uncharacterized and unknown. In the course of ontogeny, cyclins and CDKs expression and activity levels oscillate in a synchronous manner, consequently affecting CMs proliferation ability. Cyclins-CDKs expression levels reach a peak at E12 approximately, decreasing until P0 causing a concomitant decline in CMs proliferation, as demonstrated by Western blot analysis in Ikenishi et al. (2012) report (Ikenishi et al., 2012). In the timeframe surrounding P5, CMs terminally differentiate and undergo

binucleation and many cell cycle-related mediators and inhibitor are upregulated, namely (Pasumarthi & Field, 2002; Ikenishi et al., 2012; Mahmoud et al., 2013; Tane et al., 2014a). From this point onwards, a progressive downregulation of the expression and activities of cyclins and CDKs is observed. This is associated with silencing of cell cycle-related and cytoskeleton organization-related genes leading to cell cycle arrest, as shown by microarray analysis in Gan et al. (2015).

During embryonic and early neonatal development, both DNA replication and cytokinesis occur in the vast majority of CMs (Fig.5A). Terminal differentiation causes cytokinesis blockage leading to binucleation, and distinct mechanisms have been proposed to explain this failure: (1) sarcomeres incomplete disassembly due to gradual increased complexity along CMs maturation, physically impairing the separation of daughter cells (Fig.5B) (Li et al., 1997a; Li et al., 1997b); (2) incorrect formation of the contractile ring and assymetric furrow ingression due mislocation to the midbody of anillin, which is diffusely located in the cell cortex and hinders proper abscission (Fig.5C) (Engel et al., 2006). Recent work by Naqvi et al. (2014) suggested that binucleated CMs are able to successfully undergo cytokinesis. The mechanisms underlying this division are however not totally understood (Naqvi et al., 2014).

Our understanding of the mechanisms underlying CMs proliferation has increased significantly in recent years. During murine development these cells gradually cease to proliferate as they terminally differentiate. This also includes the transition from a round to rod-like cellular morphology, multinucleation and cell cycle withdrawal. Despite being commonly accepted that CMs withdraw from the cell cycle shortly after birth, progression through the cell cycle and its duration remain largely unknown. Furthermore, the association between CMs' morphometry and cell cycle status is also poorly characterized and it may unveil some clues about the proliferation cessation during mammalian ontogeny.

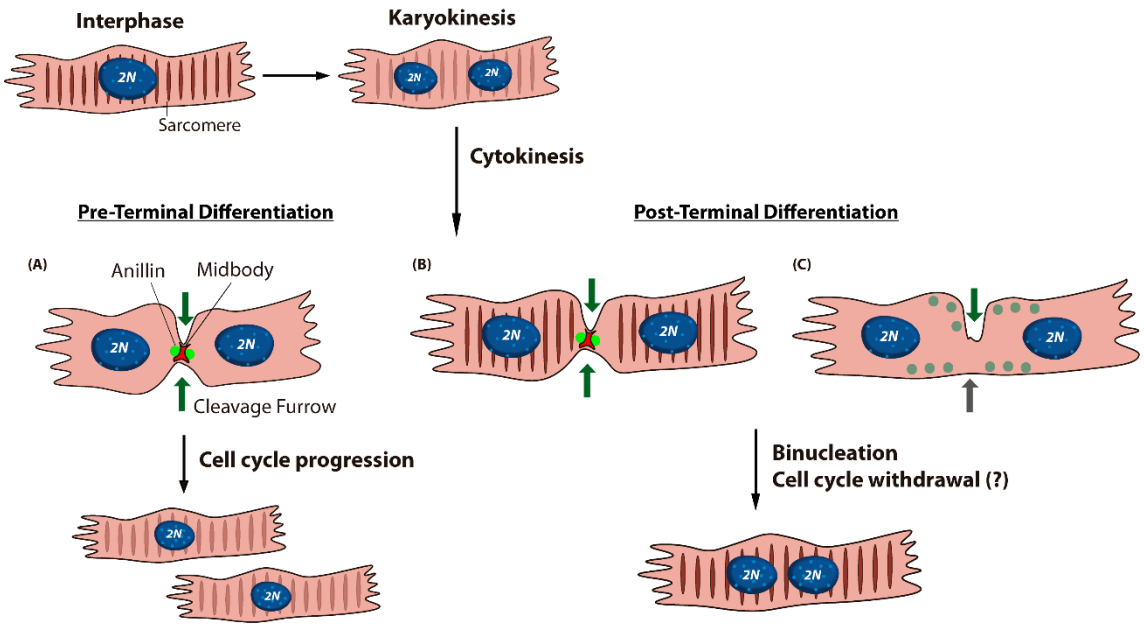

Fig.5 - Possible scenarios for cytokinesis occurrence in murine CMs. (A) Embryonic and neonatal CMs undergo successful cytokinesis which includes full sarcomeres' disassembly, correct furrow ingression and positioning of anillin in the midbody, forming two mononucleated diploid (2N) CMs. Terminally differentiated CMs fail cytokinesis due to (B) sarcomere incomplete disassembly resulting in binucleated CMs, or (C) incorrect formation of the contractile ring and assymetric furrow ingression due to mislocation of anillin.

AIMS

Current regenerative strategies based on proliferation of cardiomyocytic progenitors has so far delivered modest results. Therefore the current main focus of research turned to the development of approaches to trigger renewal of preexisting CMs and/or to increase cardiomyogenic precursor cells activity. However, there are several inconsistencies and unanswered questions in the field, which are mainly related with technical difficulties such as efficient isolation of intact CMs and lack of CMs markers. In this context, deeper insight on CMs maturation and proliferation is essential. Thus, the herein research work aimed to:

i. perform a detailed characterization and quantification of CMs' nuclei and morphometric dynamics throughout embryonic, early postnatal and adult murine life.

ii. evaluate cell cycle status and proliferation of CMs within the developing murine heart, in the course of ontogeny.

The knowledge here acquired will provide new insights on the events underlying CMs maturation and development, allowing to develop tools to identify dividing CMs and to launch novel studies regarding the proliferation cessation and cell cycle withdrawal phenomena. This work also intends to overcome technical limitations related with the isolation and characterization of developing CMs, which has been hindering further studies in this area. The identification of a stable and small fraction of immature and putatively mitotic competent CMs within the heart is thus of potential therapeutic interest, providing the basis for further studies.

MATERIALS & METHODS

Animal model: C57BL/6J mice

C57BL/6J mice (*Mus musculus*) were bred and maintained at the IBMC·INEB Animal Facility in accordance with animal care and bioethical committee guidelines. All experiments involving animals were done in compliance with the relevant laws and institutional guidelines and were approved by local and European ethic committees (Directive 2010/63/EU).

Harvesting and flash-freeze of murine hearts

Embryonic stages

To collect E10.5, E13.5 and E17.5 murine hearts, timed-pregnant females were used (the day of the vaginal plug was designated E0.5). For embryo dissection, the mother's abdomen was opened to expose the uterine horns, which were excised to a Petri dish with ice-cold phosphate-buffered saline (PBS). Under a stereomicroscope (Olympus SZX-FOF coupled to a Olympus KL 1500 LCD light source) and using fine forceps, decidua were isolated and the uterine muscular wall, Reichert's membrane and visceral yolk sac were separated from the actual embryo (Fig.6). After harvesting, hearts were immediately flash-frozen in liquid nitrogen stored at -80ºC.

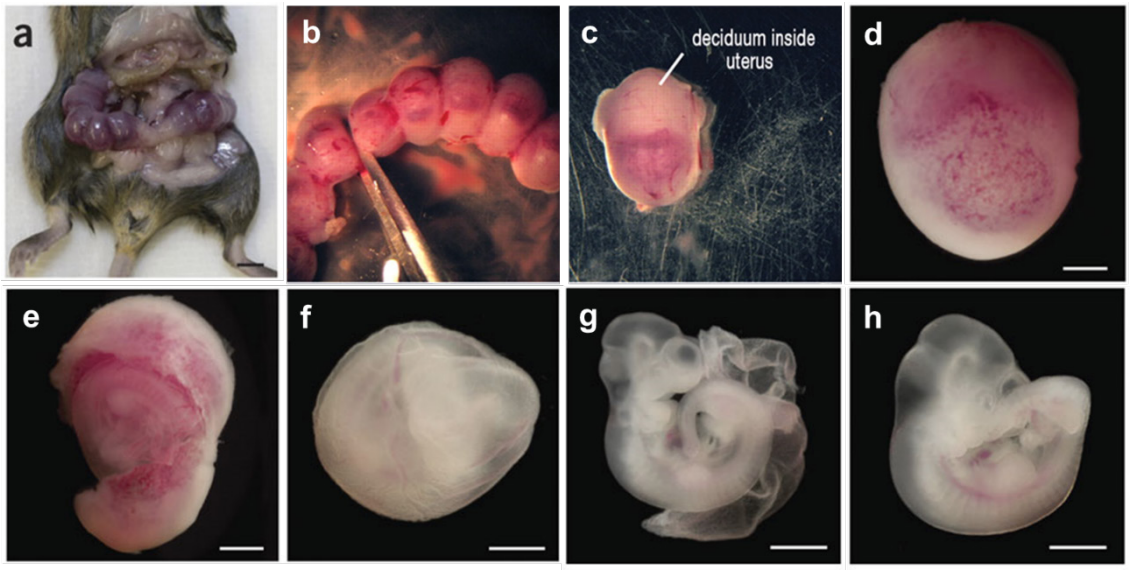

Fig.6 - Dissection procedure of E10.5 embryo for heart harvesting. (a) After opening the abdominal cavity of the time-pregnant female, the uterine horns are carefully pulled out with forceps. Scale bar: 0.5 cm. (b,c) Decidua are then separated with scissors, and the embryo is removed with the placenta and yolk sac attached and intact (d). (e) Placenta

and Reichert's membrane surrounding the yolk sac are torn open. (f,g,h) To isolate the embryo, the yolk sac is then torn open with fine forceps, and the heart is harvested. Scale bar in d-g: 1 mm. Adapted from Boisset et al. (2011).

Postnatal and adult stages

After euthanasia of postnates' (P0, P3, P7, P10, P15 and P24), hearts were harvested and placed on ice-cold cardioplegic solution (4 mM KCl in PBS) to accomplish asystole. Adult hearts were either collected and placed in ice-cold cardioplegic solution or perfused with 4% (v/v) paraformaldehyde (PFA). For cardiac perfusion, the animal was firstly anesthetized via intraperitoneal injection of 0,17mg/30g sodium pentobarbital. Once the animal became unconscious, the abdomen was opened to expose the inferior/caudal vena cava, where a catheter, connected to the peristaltic pump, was placed to perfuse with PFA for 15 min. To assure proper perfusion, the portal vein was also cut. The heart was then collected and placed on ice-cold PBS.

After removing the associated vessels and fat, the tissue was minced in approximately 2 mm^2 blocks, flash-frozen in liquid nitrogen and stored at -80ºC.

Isolation of murine cardiomyocytes

For CMs isolation, flash-frozen tissue was first fixed in 4% (v/v) PFA, at room temperature (RT) for 2 hours while stirring (≈ 110 rpm). After rinsing once with PBS for 5 min, the tissue was enzymatically digested overnight (ON), at 37ºC on a rotator (110 rpm), with 3 mg/mL collagenase type II (Worthington) in Hank's Balanced Salt Solution with Ca^{2+} and Mg^{2+} (HBSS, Sigma-Aldrich). Once full digestion was achieved, HBSS supplemented with 10% fetal bovine serum (FBS, Gibco) solution was added to inhibit collagenase activity. Next, a 390*g* centrifugation for 10 min at 4ºC was performed and cells were ressuspended in 3% FBS in PBS. Cells were counted in a hemocytometer.

CMs cytospins: immunocytochemistry and analysis

Enzymatically dissociated CMs' preparations (Table 1) were centrifuged at 239*g* for 7 min, ressuspended in 10% FBS in PBS and cytospun (Shandon Cytospin®, Thermo) for 5 min at 130*g* onto Superfrost® Plus slides (VWR).

Table 1 - Optimal CMs suspensions' cell density for cytospin smears.

Mouse ontogenic stage	Optimal CMs density per staining
E10.5 - E17.5	0.15 x 10^6 cells
P0 - P10	0.05 x 10^6 cells
P15 - Adult	0.01 x 10^6 cells

Afterwards, a permeabilization step with 0.5% Triton X-100 in PBS was performed for 7 min, in case of intracellular/nuclear antigens' staining. Primary (Table 2) and secondary antibodies were diluted in 3% FBS in PBS or in 0.02% Tween-20 in PBS, if permeabilization was required. The primary antibody incubation was carried out for 1-2 hours on ice. After three washes with the antibody diluent, 1 min each, incubation with secondary antibodies (1:1000, Life Technologies) was performed for 1 hour on ice. DNA was stained with 4'6-diamidino-2-phenylindole (DAPI) (1:10000, Vector Laboratories), and the slides mounted in mounting medium containing 2.5% (m/v) n-propyl-gallate (Sigma-Aldrich) in 10% PBS and 90% glycerol.

Representative images were acquired on Axiovert 200M inverted fluorescence microscope (Zeiss) (63x and 100x magnitude) and ImageJ® (FiJi 1.49t) was used to measure the cells' area, maximal (corresponding to the major axis) and minimal (corresponding to the minor axis) feret diameters and aspect ratio (ratio of the major axis to the minor axis).

ImageStream^X: immunocytochemistry

Cardiomyocytes' suspensions (with ≈0.5x10^6 cells) were plated on a 96-well plate, centrifuged at 424.84g for 1 min and ressuspended in 3% FBS in PBS. Antibodies were diluted in this buffer: primary antibody's (Table 2) incubation was carried out for 2 hours, on ice, followed by secondary antibodies for 40 min. The secondary antibody was chosen considering the detection channels available for the ImageStream^X system. Stained cells were ressuspended in PBS until analysis. Non-stained and single-stained controls were also included for spectral compensation. For nuclear staining, far-red fluorescent nuclear DNA dye DRAQ5® (200 μM, Biostatus) was added to the samples prior acquisition.

Table 2 - List of primary antibodies used for immunocytochemistry (ICC) and immunohistochemistry (IHC), with the specific experimental conditions.

	Primary Antibody	Target	Isotype	Dilution	Permeabilization	Blocking	Antibody Diluent	Incubation time	Secondary Antibody Incubation
ICC	Sarcomeric α-Actinin (A7811, Sigma-Aldrich)	CMs' sarcomeres (Z-lines)	Mouse IgG	1:600	-	-	0.02% Tween-20 in PBS	1-2h, on ice	40min, on ice
	Phospho-Histone H3 (Ser10; pH3) (#3377, Cell Signaling)	Proliferation marker (mitosis)	Rabbit IgG	1:800	0.5% Triton X-100 7 min				
IHC	Sarcomeric α-Actinin (A7811, Sigma-Aldrich)	CMs' sarcomeres (Z-lines)	Mouse IgG	1:500	-	Mouse Ig Blocking Reagent (M.O.M., Vector Laboratories)	1% BSA + 4% FBS in PBS	ON, 4ºC	1h, RT
	Phospho-Histone H3 (Ser10; pH3) (#3377, Cell Signaling)	Proliferation marker (mitosis)	Rabbit IgG	1:800	1% Triton X-100 5 min				
	Ki67 (ab15580, abcam)	Proliferation marker (G1, S, G2, mitosis)	Rabbit IgG	1:200	0.2% Triton X-100 5 min				
	CD45 (AF114, R&D Systems)	Nucleated hematopoietic cells	Goat IgG	1:300	-				
	Connexin-43 (ab11369, abcam)	CMs' gap junction protein	Goat IgG	1:400	-	1h, RT			
	Laminin (L9393, Sigma-Aldrich)	Extracellular matrix glycoprotein	Rabbit IgG	1:350	-				

ImageStream^X: CMs' quantification and morphometric characterization

ImageStream^X (Amnis Corporation) was used for imaging cells (fluorescence and brightfield) with 40x magnification through a 488nm-laser excitation line. INSPIRE™ (Amnis) software was used for sample acquisition and IDEAS™ (Amnis) for data processing and analysis. Cell classifiers of 100 μm^2 (for embryonic stages) and 150 μm^2 (for postnatal stages) were set on the area-lower limit of all the imagery channels, during data acquisition of a minimum of 50000 events.

After acquisition, analysis is initiated with the gating of the sampled cell population for the actinin$^+$ population, which corresponds to the percentage of cardiomyocytes present in the sample (Fig.7A). Cell populations were then hierarchically gated for single-cells (excluding doublets and clusters) that were focused (Fig.7B) and were actinin$^+$/DRAQ5$^+$, to which the analysis' template was applied (Fig.7C). Cells were also classified as "round" or "rod" whether its minor axis:major axis ratio was higher or lower than 0.55 respectively. The multi-parametric analysis is based on masks, in which a set of pixels is defined for a specific region of interest (e.g. nucleus and cytoplasm) and used to calculate feature-specific values from the acquired imagery. On the brightfield single images, masks (function "morphology mask") delimiting the entire cellular area were created, to calculate the CMs' area, major and minor axes and the proportion of round and rod-like shaped cells. The number of nuclei was manually calculated using the imagery obtained with ImageStream^X system.

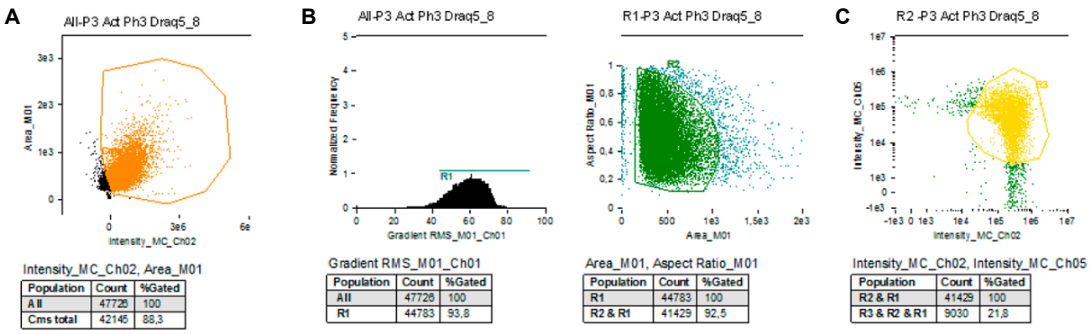

Fig.7 - Identification of CMs using IDEAS™ (Amnis) software. (A) The percentage of CMs present in the cell suspension was determined based on the frequency of Actinin expression. (B) Gating strategy used to exclude events that were not in focus (left panel) and cell doublets (middle panel). (C) To select the CMs population for further analysis actinin$^+$/DRAQ5®$^+$ subpopulation was selected (right panel).

Gelatin embedding of murine hearts for Cryosectioning

To perform immunohistochemistry (IHC), murine hearts were embedded in gelatin for cryosectioning. Hearts were fixed ON at 4ºC in 0.2% (v/v) PFA in 0.2 M phosphate buffer (PB - 0.2 M Na_2HPO_4 and 0.2 M $NaH_2PO_4 \cdot H_2O$) with 0.12 mM $CaCl_2$ and 4% sucrose. In the following day, hearts were transferred to PB with 4% sucrose, and then to PB with 15% sucrose, with both incubations being carried on ON at 4ºC. Hearts were then incubated in PB with 15% sucrose and 7.5% gelatin for 1 hour at 37 ºC, after which they were transferred to an embedding mold filled with warm gelatin solution, to be frozen in dry ice-chilled isopentane and stored at -80 ºC, until sectioning.

Gelatin-embedded hearts were cut longitudinally on a cryostat (Microm HM550, Thermo Fisher Scientific), into 5 µm-thick serial sections collected on Superfrost® Plus slides, air-dried for at least 30 min, and then stored at -80 ºC.

Immunohistochemistry

Heart cryosections were washed three times in PBS, 5 min each wash, and permeated for 5 min with Triton X-100: a final concentration of either 0.2% or 1% was used for cell membrane or cytoplasmic staining and intra-nuclear staining, respectively. Sections were blocked with Mouse Ig Blocking Reagent (Vector Laboratories) for 1 hour at RT. Antibodies (Table 2) were diluted in 1% bovine serum albumin (BSA) with 4% FBS in PBS. Primary antibody incubation was made ON at 4°C, followed by washes with PBS and a 1 hour-incubation at RT with the corresponding secondary antibodies (1:1000, Life Technologies), both in humid chambers. Slides were then mounted with Fluoroshield™ (Sigma-Aldrich) mounting medium with DAPI, and sealed after cover-slipping.

Image acquisition was performed using IN Cell Analyzer 2000® system (GE Healthcare) (20x and 40x magnification). The obtained imagery was used to quantify the number of cell cycle active (Ki67-expressing) and mitotic (pH3-expressing) cells within the CMs population along ontogeny. Direct counting was performed on ImageJ/Fiji® software, and the numbers were expressed *per* mm^2 of whole-heart, atria or ventricle.

Data and statistical analysis

Statistical analysis was performed with SPSS® Statistics v22.0 (IBM). After testing for normality, Kruskal-Wallis test (for non-parametric data), one way analysis of variance (ANOVA) with post hoc Tukey's test and Student’s unpaired t-test (both for parametric data) was chosen as appropriate, to determine whether differences between the groups were significant. $p \leq 0.05$ was considered statistically significant. Data are presented as mean ± standard deviation (SD).

RESULTS

CMs' morphometric and nuclear dynamics: characterization along ontogeny

Heart development entails a gradual increase of the tissue's complexity, as the cellular diversity increases and CMs enlarge and mature. As the heart matures, CMs' cytoarchitecture undergoes drastic rearrangement. This event results in the sarcomeres' assembly, transition from a round to a rod-like morphology and the formation and reorganization of intercalated discs (ICD) to the cell's apical ends. This growing complexity (and thus difficulty in identifying CMs) can be easily appreciated by immunohistochemistry (IHC) in heart sections of distinct ontogenic stages. By performing IHC for CMs' cytocomponents sarcomeric α-actinin (present in the sarcomeres' Z-lines), connexin-43 (present in ICD for cell-cell contact) and laminin (a common extracellular matrix glycoprotein), the difficulties in accurately isolating CMs by identifying their borders are clear (Fig. 8). This approach has, however, been used by distinct laboratories to measure CMs and to quantify CMs number, which can lead to misestimating.

With the goal of performing a detailed characterization of CMs morphometric dynamics throughout ontogeny, we have decided to further optimize a novel protocol for isolation of CMs, based on the work of Mollova et al. (2013), in which flash-frozen heart tissue blocks are enzymatically digested with collagenase II at 37ºC, after fixing. This protocol was used to isolate CMs of distinct ontogenic stages (Fig. 9A). It allows to obtain high yield of well-isolated CMs (Fig. 9B) with intact morphology and sarcomeric apparatus, which was validated by performing cytospins of the isolated cells and immunocitochemistry (ICC) for sarcomeric α-actinin and DAPI (Fig. 9C). Cell fragmentation is observed when isolating CMs from the adult heart, as these cells are fully mature. To overcome this, we have tested different optimization steps, being that cardiac perfusion with 4% PFA provided a better preservation of the cells' integrity after enzymatic digestion (Fig. 9C). Nonetheless, further optimization is still required.

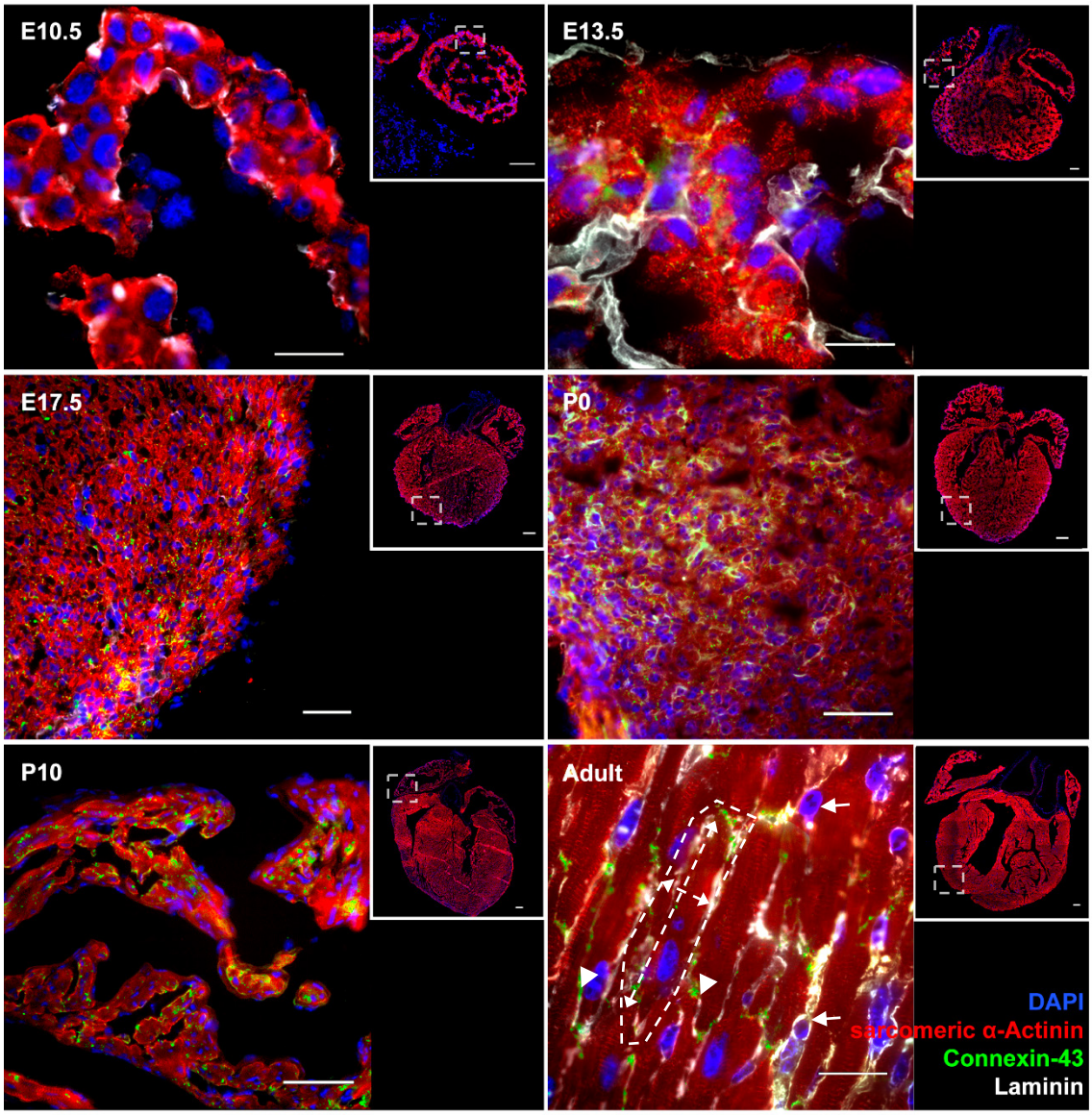

Fig.8 - Increasing complexity of the heart tissue, depicted by the distribution of gap junction protein Connexin 43 and the extracellular matrix protein Laminin, in the developing murine heart. Connexin-43 is firstly detected at E13.5 surrounding the cell membrane, whereas in the adult stage it is mainly present in the intercalated discs (arrowheads). Laminin distribution is also dynamic, as in the earliest embryonic stages is limited to patches, then concentrating around the cells' lateral borders. During heart development, CMs elongate and become tightly linked with other resident non-cardiomyocytic cells (solid arrows), hindering nuclei and cell individualization to measure the cells' dimensions (striated arrows). Representative images are provided Scale bar = 100 µm and 20 µm (inset).

The morphometry of isolated CMs was analyzed using ImageStream^X, which combines the high-throughput power of flow cytometry with high-resolution imaging, thus allowing automatic acquisition of statistically robust data of a variety of cellular parameters. This strategy allowed analyzing a high percentage of CMs from each stage analyzed, which were identified based on actinin expression (see methods for detailed gating information) (Fig.10A,B).

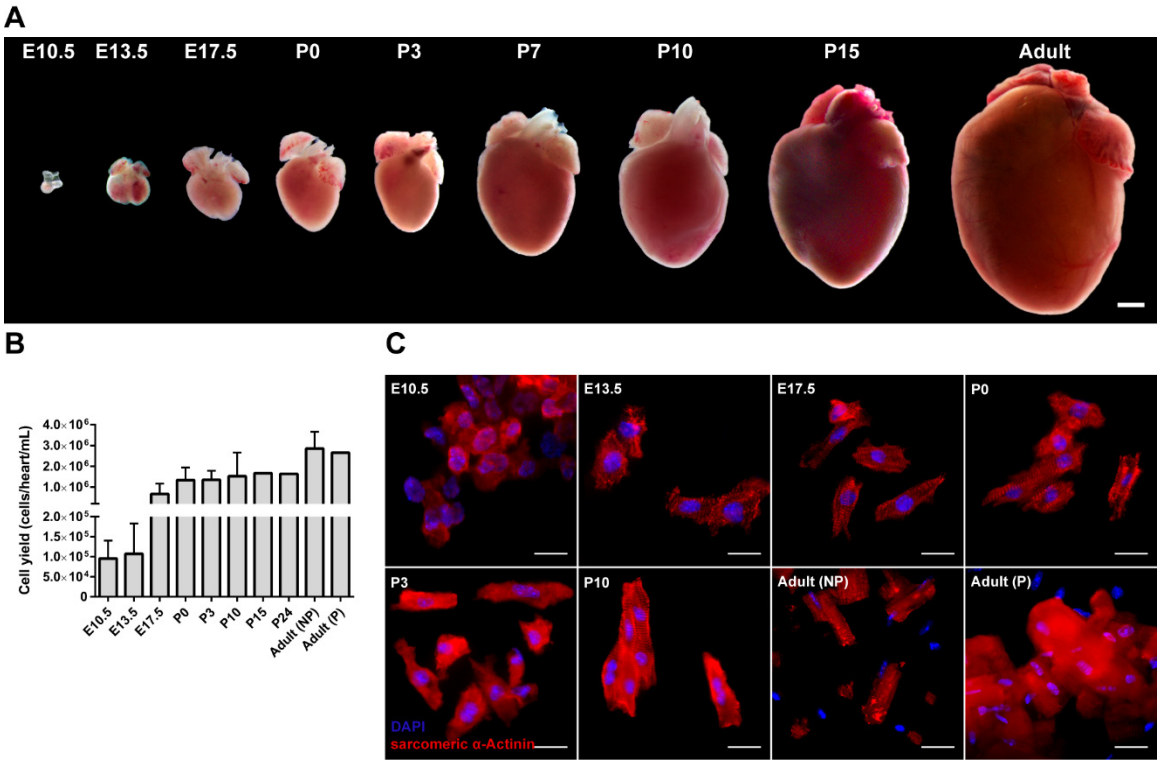

Fig.9 - Optimization of CMs isolation from the adult murine heart. (A) Murine cardiac development, from the rightward-looped linear tube (E10.5) to the fully developed four-chambered adult heart. Scale bar: 1 mm. (B) Cell yields obtained during isolation of CMs from developing hearts. Data shown as mean ± SD. (C) Cytospins of CMs suspensions obtained with the established isolation protocol, which results in a high yield of CMs with well-preserved morphology and sarcomeric apparatus. Perfusion with 4% PFA (P) results in CMs with better morphology than the ones obtained from non-perfused hearts (NP). CMs were identified through staining for sarcomeric-α-actinin (red) and DNA was stained with DAPI (blue). Scale bar: 20 μm. n(replicates):10,9,15,7,6,2,1,1,6,1 and details for replicability can be found in Supplementary Table 1.

We have evaluated several cellular morpho-parameters, such as major and minor axes, area and aspect ratio (AR). Regarding cell aspect ratio, in the earliest stages analyzed (E10.5), the majority of CMs present a round morphology (~80%) (Fig.10C), corresponding to an AR of 1:1, as expected (Fig.10D,E). The remaining cells were considered to be elongated cells, even though they presented an immature morphology. The proportion of round CMs was maintained in fetal stages (E17.5) and decreased to about 50% following birth (P0, $p<0.05$) (Fig. 10C,D). Our data thus indicate that the beginning of the shift in the cells' morphology occurs around birth (E17.5-P0), with the cells undergoing elongation, showing an AR of 2:1 or 3:1 (Fig.10C, D and E). Our analysis also evidenced the presence of a small fraction of round-shaped CMs at late ontogenic stages (Fig.10C, D and E), which were confirmed to be intact cells and not artifacts or fragmented cells. In the time-range here evaluated, the cells' major axis almost doubled (~25 μm to ~47 μm, $p\leq0.0001$), while minimal change in the cells' minor axis was observed (~15 μm to ~22 μm), leading to a rod-shape morphology (Fig.10F

and E). Subsequently the cell area increased by almost three-fold, from ~280 μm^2 to ~775 μm^2 (p≤0.001).

Regarding CMs' nuclear dynamics, ImageStream^X automatic analysis was not totally conclusive, as the software could not fully distinguish nuclei inside intact CMs from the ones existent in the cells' surroundings resultant from fragmented cells. For this reason, we have manually quantified the number of nuclei using the obtained imagery (Fig.11A and B). Our data shows multinucleation as starting around E17.5, with ~2% of the cells presenting two nuclei until P3 (Fig.11B). On the last time-point analyzed, P10, almost half of the cells (~48%) possess a single nucleus and the other half is multinucleated, presenting three (~1.5%) and four nuclei (~1%) (Fig. 11B). Interestingly, our analysis also evidenced a small subpopulation of mononucleated CMs that persist in the adult heart (Fig. 11B). Quantitative data for this stage is not presented due to the above mentioned difficulties in correctly isolating these cells.

ImageStream^X analysis relies on user-defined masks outlining the pixels on which a given measurement will be made. To validate this automated tool, we manually validated the obtained results by immunocytochemistry on cytospun CMs with subsequent cell dimensions' assessment using ImageJ/Fiji® software. In the time-range here assessed (E10.5-P10) our measurements confirmed an elongation event during CMs' maturation. The major axis values increased by almost two-fold, from ~27 μm to ~48 μm from E10.5 until P10 (p≤0.001). No substantial change (~16 μm to ~19 μm) was detected in the minor axis. The cell area doubled during the analyzed time-frame, from ~297 μm^2 to ~646 μm^2 (p≤0.0001) (Fig.12A). Concerning CMs aspect ratio, in E10.5, the earliest embryonic stage here analyzed, both round (AR of 1:1 ~40%) and rod-shaped (AR higher than 1:1 ~60%) CMs were detected. In the last ontogenic stage here assessed (P10) the majority of the cells display high aspect ratios, related with rod-morphology (~86%) and a small subset (~14% at P10) of round-shaped CMs with AR of 1:1 (Fig.12B). Thus, the morphometric parameters evaluated (major and minor axes, aspect ratio and area) accurately resemble the ones obtained via ImageStream^X automatic analysis.

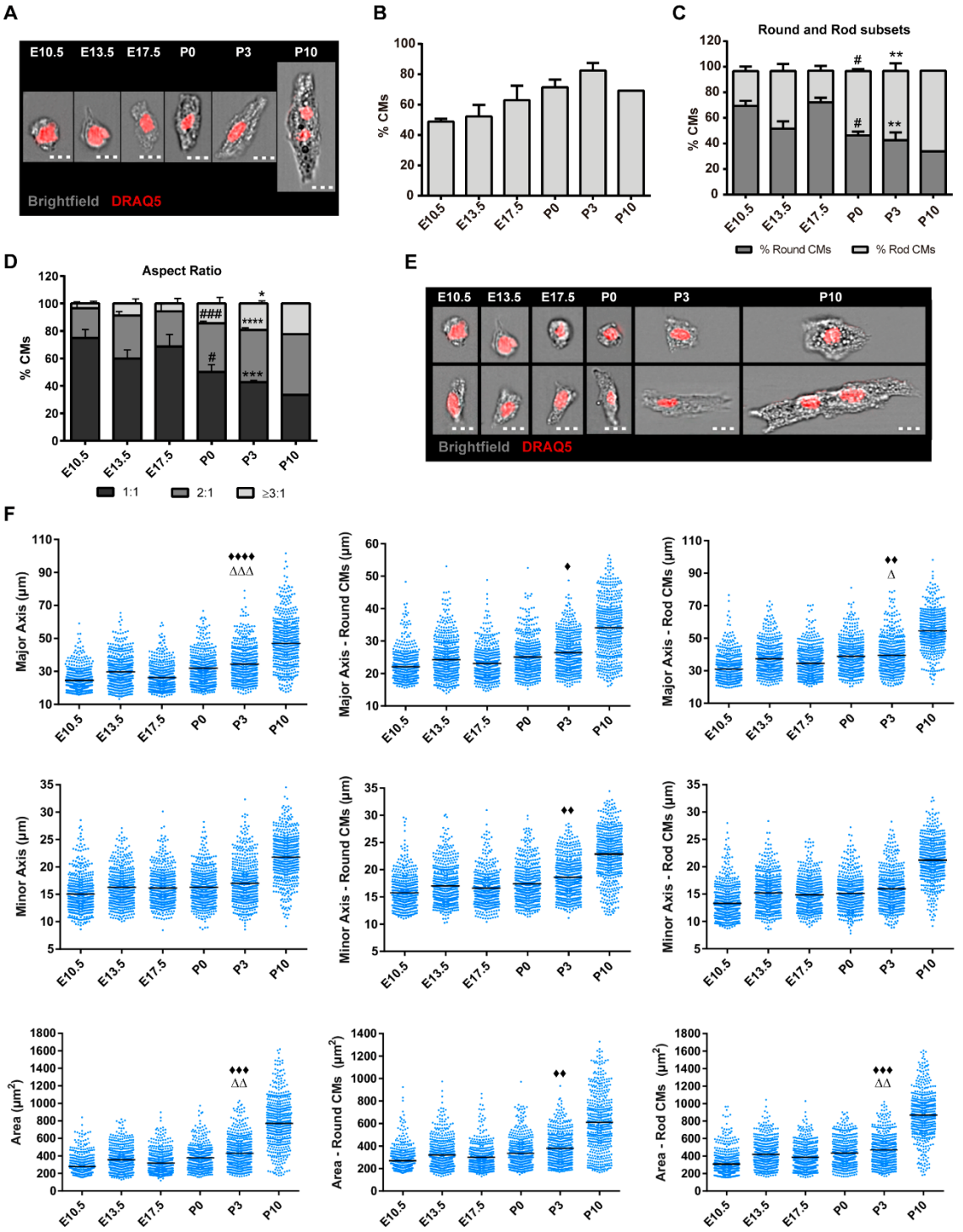

Fig.10 - ImageStream^X morphometric characterization of maturing CMs, obtained with the established isolation protocol. (A) Representative images of the CM analyzed using imaging flow cytometry; Scale bar: 10 µm. (B) CMs yield of the sampled suspensions. (C) Proportion of round and rod-shaped CMs throughout ontogeny. # $p \leq 0.05$ vs. E17.5; ** $p \leq 0.01$ *vs.* E10.5. (D) Dynamics of CMs aspect ratio along ontogeny. # $p \leq 0.05$ vs. E17.5, ### $p \leq 0.001$ vs. E17.5; * $p \leq 0.05$ *vs.* E10.5, *** $p \leq 0.001$ vs. E10.5, **** $p \leq 0.0001$ vs. E10.5. (E) Representative images of round and rod-shaped CMs along ontogeny; Scale bar: 10 µm. (F) Analysis of morphometric parameters of the whole CM population and of the round and rod-shaped subsets. For purposes of illustration, only 500 randomly chosen events are represented, with the mean values corresponding to the total dataset. ♦, P3 *vs.* E10.5; Δ, P3 *vs.* E13.5. ♦,Δ $p \leq 0.05$; ♦♦,ΔΔ $p \leq 0.01$; ♦♦♦,ΔΔΔ $p \leq 0.001$; ♦♦♦♦ $p \leq 0.0001$ by one-way ANOVA with *post hoc* Tukey's test (C,F) or Kruskal-Wallis test (D). Data are shown as mean ± SD. n(assays)=4,3,6,4,3,1.Details for replicability can be found in Supplementary Table 1.

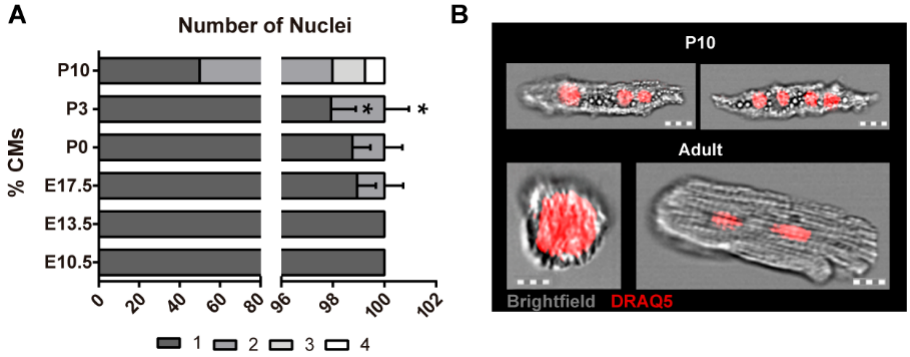

Fig.11 - CMs nuclear dynamics characterization along ontogeny. (A) Assessment of the number of nuclei per CMs obtained by direct counting using ImageStream^X imagery. * $p \leq 0.05$ *vs.* E10.5 or E13.5, one-way ANOVA with *post hoc* Tukey's test. (B) Representative images of multinucleated P10 cells, and mono- and binucleated adult CMs. Data presented as mean ± SD. n(assays)=4,3,6,4,3,1 (A). Details for replicability can be found in Supplementary Table 1.

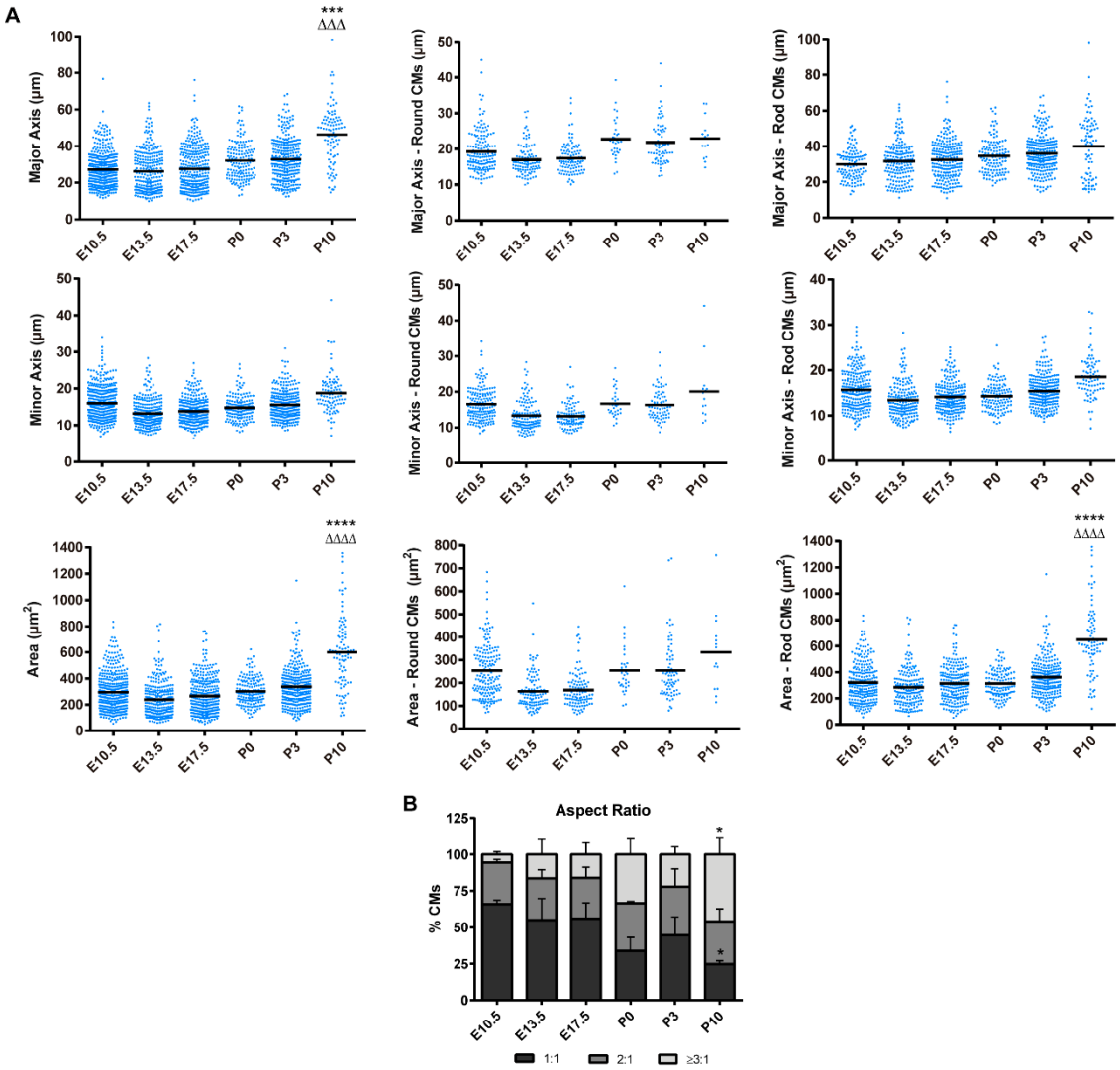

Fig.12 - Assessment of cellular dimensions during embryonic and early postnatal development in cytospins of maturing CMs. (A) Analysis of the morphometric dynamics of the total CMs population and of the round and rod-shaped subpopulation. *, P10 *vs.* E10.5; Δ, P10 *vs.* E13.5. , ***,ΔΔΔ $p \leq 0.001$, ****,ΔΔΔΔ $p \leq 0.0001$. (B) Round (AR ≤ 1:1) and rod-shaped (AR = 2:1 and ≥ 3:1) CMs proportions throughout ontogeny. * $p \leq 0.05$ *vs.* E10.5. Data are shown as mean ± SD. n(assays)=4,3,6,4,3,1. Statistical significance evaluated by Kruskal-Wallis test (A) and one-way ANOVA with *post hoc* Tukey's test (A,B). Details for replicability can be found in Supplementary Table 1.

Characterization of CMs' proliferation dynamics along ontogeny

To assess the CMs' cell cycle status and proliferation dynamics during development and determine the localization of proliferative CMs within the murine heart, we evaluated by IHC the expression of the classic proliferation markers Ki67 and phosphorylated-Histone H3 (pH3). Ki67 is a nuclear protein expressed during all the cell cycle active phases and absent in G0 (Gerdes et al., 1984). The phosphorylation of histone H3 marks the onset of mitosis (Goto et al., 2003). CMs were identified based on their specific staining for sarcomeric α-actinin. As the heart encompasses several other non-cardiomyocytic cells, such as hematopoietic cells (namely precursors of erythrocytes, leukocytes, macrophages and lymphocytes), which exhibit high rates of proliferation in the course of ontogeny (Orkin & Zon, 2008), CD45 marker was used to exclude the hematopoietic cardiac subpopulation from the analysis, avoiding overestimation of the proliferative CMs fraction (Fig.13).

The frequency of Ki67 and pH3-expressing cells was then quantified by direct counting on the whole-heart, ventricles and atria (Fig.14). With this approach we quantified whole heart and CMs proliferation levels (Fig. 14A,B). During embryonic development (E10.5-E17.5) about 30% of CMs were Ki67 and ~15% pH3-positive in the whole-heart. At birth (P0), ~50% of CMs were Ki67-positive, while ~10% expressed pH3. Afterwards, a rapid decline of the cell cycle and mitosis-active CMs was observed until adulthood, in which ~0.26% and ~0.11% of CMs were Ki67 and pH3-positive respectively (Fig.14A). To complement this analysis, we evaluated the cell cycle status and proliferation rate within the cardiac chambers (Fig.14C,D). During prenatal development, the ventricles presented an increasing CMs proliferative activity, with rates of cell cycle active and mitotic CMs ranging between 25-50% and 9-12%, respectively (Fig.14C). The proliferation rate in the ventricular wall and atria then decreases steadily in the late postnatal stages, stabilizing below 0.3% in the adulthood (Fig.14C,D). Interestingly, two peaks of proliferation were detected in the atrial cardiomyocytic population, at E13.5 and P0. In the ventricles, proliferation levels were maintained from E13.5 to E17.5 and peaked also at P0 (Fig.14B).

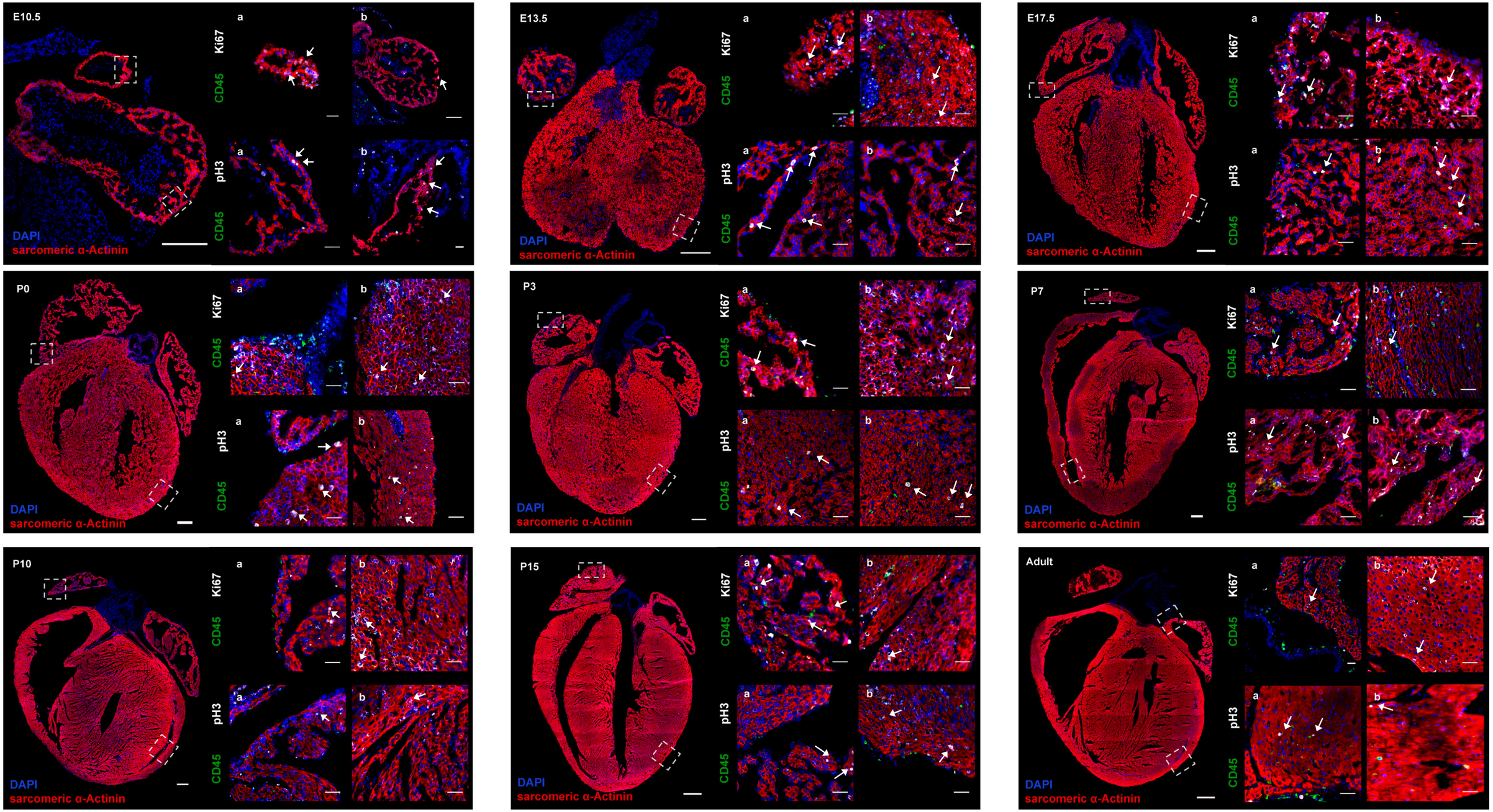

Fig. 13 - CMs' cell cycle and proliferation dynamics throughout murine ontogeny. Assessment of Ki67-expressing (white) or pH3-expressing (white) CMs, which were identified though staining of the sarcomeric-α-actinin (red). CD45 staining (green) defines hematopoietic cells. Nuclei are counterstained with DAPI (blue). Representative images are provided and arrows point at Ki67 and pH3-positive CMs. Scale bars: 100 μm (E10.5-P10 whole-heart), 250 μm (P15-Adult whole-heart) and 50 μm (inset).

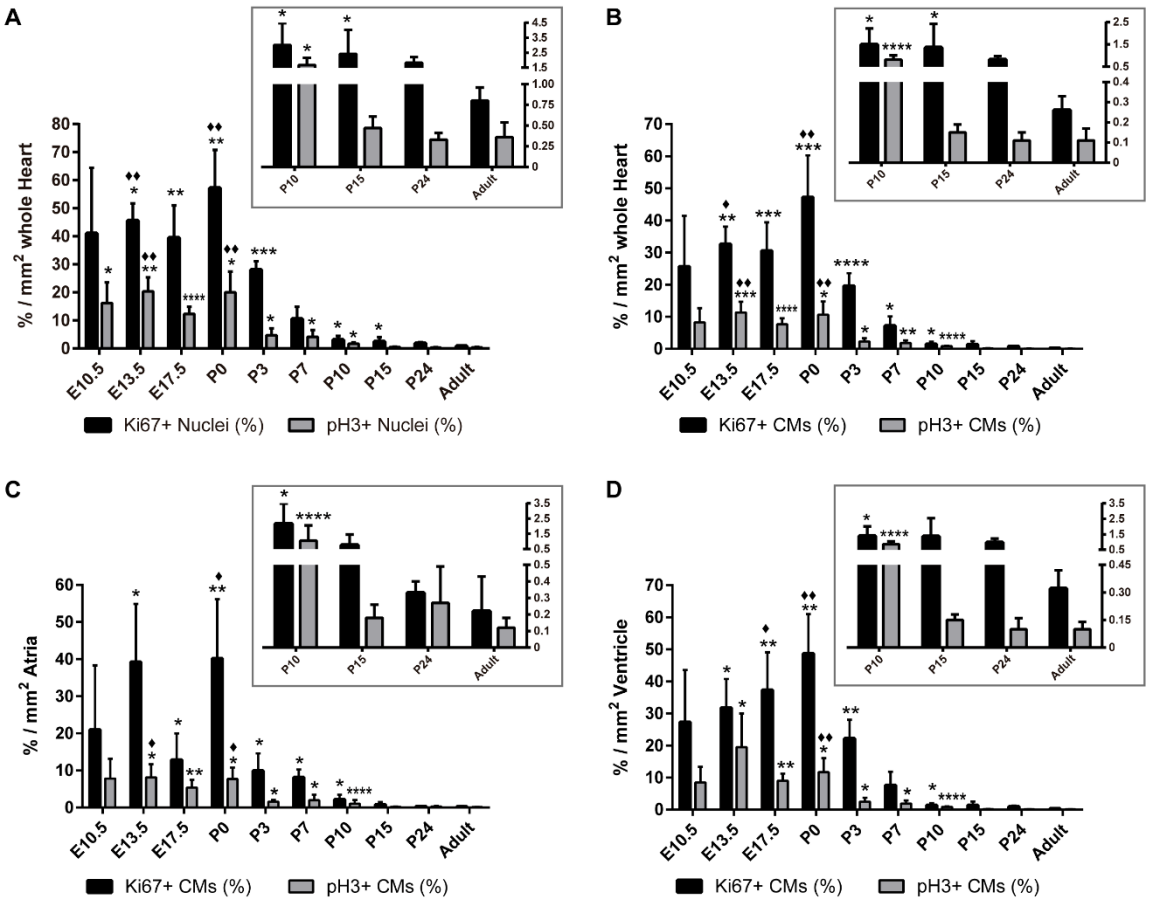

Fig. 14 - Quantitative data of CMs' proliferation and cell cycle status along murine ontogeny. Cell cycle active and proliferating total nuclei (A, Nuclei^{+}) or CMs (B,C,D, CMs^{+}) were assessed within the tissue by analyzing Ki67 and pH3 expression, respectively, followed by direct counting on the whole-heart (A,B), atria (C) and ventricles (D) Inset graphs show in more detail the quantitation of the late ontogenic stages (P10 to adult), portraying the small extent of cell cycle active and mitotic CMs within heart. Data are expressed as the mean percentage of Ki67 and pH3-positive nuclei/CMs per square millimeter of whole-heart/atria/ventricle ± SD. n=4 distinct hearts were analyzed for each stage, except for P24 in which only 2 hearts were evaluated. * *vs.* Adult, ♦ *vs.* P7.*,♦ $p \leq 0.05$, **,♦♦ $p \leq 0.01$, *** $p \leq 0.001$, **** $p \leq 0.0001$ by Kruskal-Wallis test. Details for replicability can be found in Supplementary Table 1.

Due to the difficulties in accurately identifying CMs within the tissue, we validated the data obtained, through ICC on cytospun CMs for pH3 and sarcomeric-α-actinin and observed a decreasing number of mitotic CMs from E10.5 until E17.5 (Fig.15A,B). Even though preliminary, our results indicate that the followed staining strategy and quantification using IN Cell Analyzer 2000® constitutes a good tool to quantitate CMs' proliferative extent.

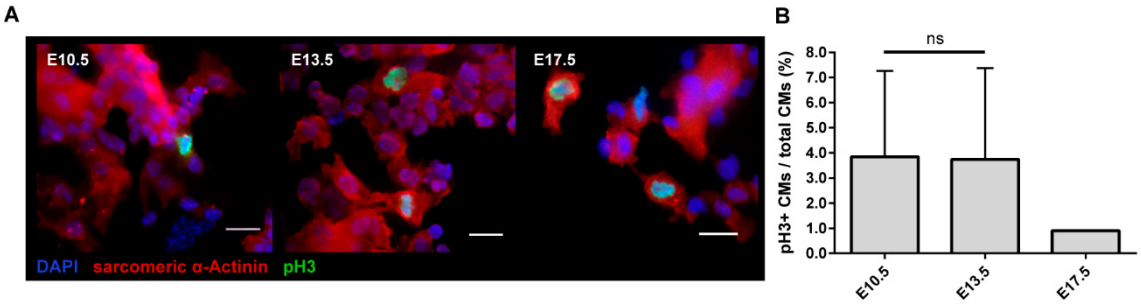

Fig.15 - Immunocytochemical assessment of proliferation in cytospins of embryonic CMs. (A) CMs were identified by sarcomeric-α-actinin staining (red) and analyzed by immunofluorescence for mitosis (pH3, green). Representative images are provided and the arrows point to proliferating CMs; Scale bar: 20 μm. (B) Quantification was made by direct counting of proliferating embryonic CMs in the total cell population and in the CMs subpopulation. Data presented as mean ± SD. n(assays)=3,3,1. Statistical significance was assessed with unpaired *t*-test, revealing non-significant (ns) differences between stages (*t* value=0.039). Details for replicability can be found in Supplementary Table 1.

DISCUSSION

Cardiomyocytes are the key players that hold the essential task of maintaining the blood circulation, sustaining the homeostasis in vertebrates. The longstanding dogma of the postnatal mammalian heart being considered a post-mitotic organ, devoid of intrinsic regenerative capacity, has been challenged by recent reports of CMs renewal in the neonatal murine heart and in the adult human heart. Despite promising, these groundbreaking studies revealed discrepancies in CMs' renewal extent due to difficulties in recognizing mammalian CMs' nuclei, associated with the tissue's complexity and due to the absence of specific surface markers to distinguish these cells from other native cells.

As immunohistochemistry is hampered by the aforementioned hurdles, several CMs isolation protocols have been used by different laboratories, which normally include tedious protocols. However, a single universal isolation method that can be easily employed to routinely produce a large yield of high quality cells, regardless of the animals' ontogenic stage, is still needed. This necessity was the major driving force that led our laboratory to optimize a novel CMs' isolation protocol, based on the work of Mollova et al. (2013), which renders high-yield and high-quality CMs (Mollova et al., 2013). This simple and rapid protocol consists of enzymatic digestion-rounds of flash-frozen and fixed cardiac tissue blocks, until full digestion is achieved. Using this protocol we were able to obtain a high yield of intact embryonic and neonatal CMs. However in the latest ontogenic stages, namely in the adult heart, fully mature CMs become fragmented during the digestion. Therefore, in the scope of this work we tested distinct alterations in the protocol and concluded that cardiac perfusion with paraformaldehyde allowed diminishing fragmentation during enzymatic digestion. Further optimization is still required, and it may include the use of connexins' inhibitors to facilitate the cells' dissociation by loss of cell-cell contacts. With this improved methodology we intend to create a benchmark, with which a large number of intact cells can be successfully obtained along ontogeny, enabling further studies to provide valuable insights into CMs' cellular and sub-cellular physiology. Additionally, this protocol is also being used in other ongoing work in Perpétua Pinto-do-Ó laboratory with the goal of identifying specific CMs' surface markers.

The unique cytoarchitecture of CMs is drastically transformed over the course of ontogeny, from round to a fully developed rod-like shape. This correlates with cessation of the CMs' proliferation ability, multinucleation (due to cytokinesis blockage), cell cycle withdrawal and cell hypertrophy. Recently, novel players in the multifactorial network of

these events have been brought to light, such as downregulation of cyclins-CDKs and mitosis-related genes (Tane et al., 2014a; Tane et al., 2014b), epigenetics (Oyama et al., 2014) and the high oxidative damage caused by ROS production due to the *in utero* hypoxia-to-normoxia transition as uncovered by Puente et al. (2014) body of work (Puente et al., 2014). The switch from a heart developmental hyperplasia to hypertrophy has been investigated in detail by Li et al. (1996). However no data is available when considering the relationship between CMs' morphometry and proliferation ability during ontogeny. Likewise, comprehension and interpretation of the CMs' cell cycle has been extremely challenging due to the aforementioned hurdles, and consequently many aspects of CMs maturation and proliferation remain unclear. Given this gap on knowledge, we set out to perform a detailed characterization of the morphometric, nuclear, cell cycle status and proliferation dynamics of CMs, throughout the maturation of the murine heart.

We have performed a detailed analysis of the CMs' cellular dimensions in the course of ontogeny using the ImageStream^X platform, which integrates the statistical power of large sample size analysis common to flow cytometry with the morphological features obtained by microscopy. To the best of our knowledge, this is the first report taking advantage of the unique abilities of ImageStream^X technology to characterize the cells' morphometry (i.e. major and minor axes, cell area and aspect ratio) of developing murine CMs. This approach, that allows high-content and high-throughput analysis and quantification, was properly validated by manually evaluation of the same cellular morpho-parameters. The values obtained in both techniques were very similar, thus confirming ImageStream^X as a valuable tool to obtain consistent and reliable data. Our results evidence the drastic morphometric rearrangement that CMs undergo along ontogeny, with large modification of the cell's major axis and minimal variation in the minor axis and concomitant increase of the cell's area. According to Hirschy et al. (2006), this elongation phenomenon into a rod-like phenotype is consequence of rigorous alignment of the sarcomeric myofibrils to the cell's major axis, required to enhance the cells' contractile force to sustain the increasing heartbeat rate as the heart matures (Hirschy et al., 2006).

In the postnatal mammalian heart, the majority of CMs are terminally differentiated and rod-shaped and our ImageStream^X data corroborate this widely accepted knowledge. Simultaneously with the occurrence of elongation, our results regarding CMs' nuclear dynamics point to E17.5 as the starting point of the binucleation phenomenon (with ~1.5% binucleated cells). After P3 a burst of binucleation was also detected, which correlates with a final round of acytokinetic mitosis leading to cell cycle

arrest and CMs' hypertrophic growth. This contrasts with the report of Soonpaa et al. (1996) that binucleation begins at P1 with ~5% of murine binucleated CMs, followed by a dramatic increase between P4-P7 (32%-88%) (Soonpaa et al., 1996). Recently, a refined study by Raulf et al. (2015) revealed distinct binucleation indexes between the adult murine ventricles (77-90%) and atria (14%), using a novel transgenic mice model expressing a fusion protein of human histone 2B and the red fluorescence protein mCherry under the control of the CMs specific α-MHC promoter (Raulf et al., 2015). The physiological and functional importance underlying binucleation is still poorly understood, but a possible explanation is that genome multiplication promotes cell survival under stressful conditions, through activation of DNA repair and protein turnover-related genes (Anatskaya & Vinogradov, 2007), while generating higher quantities of RNA transcripts to meet the hypertrophic CMs metabolic needs (Ahuja et al., 2007).

One goal of this work was to characterize the cell cycle status and proliferation dynamics of the CMs population within the developing murine heart. Using immunohistochemical analysis, we were able to verify a gradual decrease of the cell cycle active and proliferating CMs subset from embryonic life until adulthood, consistent with the fact that CMs permanently exit the cell cycle by the end of the neonatal period, as they terminally differentiate (Walsh et al., 2010). Besides CMs, the permanent cellular constituents of the heart include cardiac fibroblasts, hematopoietic and endothelial cells and vascular smooth muscle cells. These non-cardiomyocytic lineages exhibit high rates of proliferation in the course of ontogeny, reason why its exclusion from the analysis is crucial. We used the hematopoietic cell marker CD45, and excluded cells that were circularly arranged or in large cords forming blood capillaries or vessels.

Our data is in agreement with Kosaka et al. (2012), which quantitated the extent of pH3-positive CMs in sections of E12.5 whole heart, revealing a mitotic index of ~0.02 to ~0.025 (ratio of the number of $pH3^+$ nuclei to the total number of cells in the heart) (Kosaka et al., 2012). We report a mitotic index of ~0.01% at E13.5 whole heart and demonstrate decreasing CMs proliferation with heart maturation. Analysis of proliferation in cardiac chambers only, indicated that ventricular CMs are highly proliferative. This is consistent with their function as pulmonary-systemic blood pumping chambers, requiring proper wall thickening to keep up with the growing heartbeat rate. A mitotic index of 0.01-0.02 in the E12.5 left ventricle was described by Kosaka et al. (2012), similarly to the mitotic index here obtained (~0.01) (Kosaka et al., 2012). In our analysis we identified two peaks of proliferation along mouse ontogeny: at E13.5 (atria only) and P0 (whole-heart).

The proliferative peak detected at E13.5 correlates with myocardial growth and trabeculation of the ventricular wall, which serves primarily as a mean to increase myocardial oxygenation, while the coronary circulation is not fully developed (Wessels & Sedmera, 2003). At this stage, a top-to-base gradient of increasing proliferation arises with the basal compact myocardium displaying higher proliferating activity. The compact layer is relatively thin with highly proliferative CMs in S/G2/M phases whereas the trabecular myocardium comprises terminally differentiated CMs, predominantly arrested in G0/G1 phase (Park et al., 2013). At E13.5 another complex morphogenic event occurs in the right ventricle with the formation of the infundibulum, a funnel-shaped portion of the ventricle that opens into the developing pulmonary artery (Webb et al., 1998). Atrial CMs undergo a proliferative burst related with septation of the atrial chamber by formation of the atrial muscular septum. In the end, the primitive atrial chamber becomes fully divided in two individual compartments (Webb et al., 1998; Anderson et al., 2003; Moorman & Christoffels, 2003). The coincident growth of both cardiac chambers at E13.5 is also correlated with the activation of the main cyclins and CDKs, therefore indicating an activation of the cell cycle and subsequent cell division, as reported by Ikenishi et al. (2012).

The second proliferative burst here detected occurs at the day of birth (P0), with ~50% of Ki67-positive and ~10% of pH3-positive CMs per mm^2 of tissue. This peak of mitosis correlates with the 40% increase in the CMs population number recently described by Naqvi et al. (2014) during P0 until P4 (Naqvi et al., 2014). This work assessed the total number of CMs in both ventricles during mice ontogeny, by direct counting of enzymatic isolated-derived CMs. D'Uva et al. (2015) reported 0.5%-1% of pH3-positive CMs (using IHC) in the left ventricle cells of P1 hearts,(D'Uva et al., 2015). In agreement with this, at E17.5 by ICC we detect ~0.7% pH3-expressing CMs in the total cells. Regarding Ki67 expression, at P3 our data show that ~2.5% of CMs is Ki67-positive, which is in line with the values previously obtained by flow cytometry (Walsh et al., 2010). Our findings, however, contradict Ikenishi and colleagues' work, which reported that P0 presents the minimum expression levels of cyclins-CDKs in perinatal development (Ikenishi et al., 2012). Since no major morphogenic event is described to occur in the heart at birth, the peak of proliferation evidenced at P0 at first glance seems to result from CMs developmental hyperplasia to sustain the increasing hemodynamic load. Further studies are required to better understand the perinatal CMs' proliferative burst, as it might unravel some clues about CMs' terminal differentiation and proliferation cessation. In addition, our results shows that in neonatal hearts (P3-P7) the majority of CMs have acquired a cell cycle inactive status and no longer proliferate. Nonetheless,

from P3 onwards only ~20% of total CMs retains proliferative activity in the neonatal life, which is in agreement with the narrow time-window for heart regeneration in the first week of postnatal life reported by Porrello et al. (2011) using a apex resection-model (Porrello et al., 2011).

Our data also allowed observing a modest frequency of Ki67 and pH3-expressing CMs in the late ontogeny, namely in the adult heart, in agreement with recent reports (Bergmann et al., 2009; Kajstura et al., 2010). This observation correlates well with our previous identification of a small subset of round and mononucleated CMs in late ontogenic stages, i.e. in the adult heart. These features are hallmark of embryonic myocytes. These results suggest the presence of an immature or less mature niche within the postnatal CMs pool, constituted of round mononucleated CMs, which reinforces previous studies reporting the identification of mitotic cardiac progenitors in the postnatal mammalian heart (Senyo et al., 2013). Whether these cells correspond to the small proliferative subset identified in the adult will be assessed by ImageStream^X, which we have proven to correctly distinguish round and rod-shaped CMs subsets. For this reason, the optimization of the CMs isolation protocol is crucial to obtain high cell quantity and quality in the adult stage. Additionally, evaluating the ploidy of the round mononucleated CMs here reported in the late developmental stages, would be of great interest in order to confirm if the cells are diploid, mimicking the embryonic karyotype. This would ratify once more its immatureness and potential to remain proliferative and play a role in CMs renewal in the adult mammalian heart.

Overall, in the herein work we demonstrated that ImageStream^X can be used to accurately characterize CMs morphometry along ontogeny. Combination of this high-throughput technique with immunohistochemistry allows obtaining quantitative data and cell-position information, respectively. Our approach evidenced the presence of immature or less differentiated niches of CMs within the murine heart, with features of the proliferative embryonic phenotype, such as small size, round shape and mononucleation. Characterization of these cells (and additional CMs subsets) is essential to achieve a better comprehension of CMs maturation and thus of the mechanisms underlying cell cycle blockage with differentiation. Ultimately, this will allow to understand if mature CMs can be reverted to a less mature state, re-acquiring a proliferative status.

CONCLUSIONS

Herein we aimed to characterize the dynamics of the CMs' morphometry, nuclei, and proliferation in the course of mouse ontogeny, through a combination of powerful tools. In the scope of this study, we have (i) corroborated ImageStream^X as a valuable tool for high-content CMs analysis; (ii) improved the protocol for isolation of adult CMs, diminishing their fragmentation; (iii) demonstrated CMs' elongation and binucleation starting at around E17.5, leading to fully mature rod-shaped and multinucleated cells, with up to four nuclei at P10; (iv) verified the presence of a small subset of mononucleated and round-shaped CMs in the late ontogenic stages, which may retain mitosis-competence; (iv) identified two peaks of proliferation, associated with cardiac chamber maturation; and finally, (v) confirmed a decrease in the number of cell cycle-active and mitotic CMs, during ontogeny, with a small-extent of proliferation being detected in the adulthood.

Globally, this work is a contribution towards a better understanding of the events underlying the relationship between CMs' maturation, loss of proliferation and cell cycle withdrawal in the adult mammalian heart. Comprehending these mechanisms is crucial to shed light on the CMs' cell cycle progression and withdrawal. It will also allow to verify the presence of putative niches of less-mature CMs, within the adult mammalian heart.

BIBLIOGRAPHY

Ahuja, P., et al. (2004). "*Sequential myofibrillar breakdown accompanies mitotic division of mammalian cardiomyocytes*." J Cell Sci 117(Pt 15): 3295-3306.

Ahuja, P., P. Sdek and W. R. MacLellan (2007). "*Cardiac myocyte cell cycle control in development, disease, and regeneration*." Physiol Rev 87(2): 521-544.

Anatskaya, O. V. and A. E. Vinogradov (2007). "*Genome multiplication as adaptation to tissue survival: evidence from gene expression in mammalian heart and liver*." Genomics 89(1): 70-80.

Anderson, R. H., et al. (2003). "*Development of the heart: (2) Septation of the atriums and ventricles*." Heart 89(8): 949-958.

Balmer, G. M., et al. (2014). "*Dynamic haematopoietic cell contribution to the developing and adult epicardium*." Nat Commun 5: 4054.

Banerjee, I., et al. (2007). "*Determination of cell types and numbers during cardiac development in the neonatal and adult rat and mouse*." Am J Physiol Heart Circ Physiol 293(3): H1883-1891.

Bartman, T. and J. Hove (2005). "*Mechanics and function in heart morphogenesis*." Dev Dyn 233(2): 373-381.

Beltrami, A. P., et al. (2003). "*Adult cardiac stem cells are multipotent and support myocardial regeneration*." Cell 114(6): 763-776.

Bergmann, O., et al. (2009). "*Evidence for cardiomyocyte renewal in humans*." Science 324(5923): 98-102.

Boisset, J. C., et al. (2011). "*Ex vivo time-lapse confocal imaging of the mouse embryo aorta*." Nat Protoc 6(11): 1792-1805.

Bolli, R., et al. (2011). "*Cardiac stem cells in patients with ischaemic cardiomyopathy (SCIPIO): initial results of a randomised phase 1 trial*." Lancet 378(9806): 1847-1857.

Buckingham, M., S. Meilhac and S. Zaffran (2005). "*Building the mammalian heart from two sources of myocardial cells*." Nat Rev Genet 6(11): 826-835.

Cai, C.-L., et al. (2003). "*Isl1 Identifies a Cardiac Progenitor Population that Proliferates Prior to Differentiation and Contributes a Majority of Cells to the Heart*." Dev Cell 5(6): 877-889.

Cai, C. L., et al. (2008). "*A myocardial lineage derives from Tbx18 epicardial cells*." Nature 454(7200): 104-108.

D'Uva, G., et al. (2015). "*ERBB2 triggers mammalian heart regeneration by promoting cardiomyocyte dedifferentiation and proliferation*." Nat Cell Biol 17(5): 627-638.

de Boer, B. A., et al. (2012). "*Growth of the developing mouse heart: an interactive qualitative and quantitative 3D atlas*." Dev Biol 368(2): 203-213.

Delorme, B., et al. (1997). "*Expression pattern of connexin gene products at the early developmental stages of the mouse cardiovascular system*." Circ Res 81(3): 423-437.

Drenckhahn, J. D., et al. (2008). "*Compensatory growth of healthy cardiac cells in the presence of diseased cells restores tissue homeostasis during heart development*." Dev Cell 15(4): 521-533.

Driesen, R. B., et al. (2009). "*Re-expression of alpha skeletal actin as a marker for dedifferentiation in cardiac pathologies*." J Cell Mol Med 13(5): 896-908.

Engel, F. B., M. Schebesta and M. T. Keating (2006). "*Anillin localization defect in cardiomyocyte binucleation*." J Mol Cell Cardiol 41(4): 601-612.

Field, C. M. and B. M. Alberts (1995). "*Anillin, a contractile ring protein that cycles from the nucleus to the cell cortex*." J Cell Biol 131(1): 165-178.

Freire, A. G., T. P. Resende and P. Pinto-do-Ó (2014). "*Building and repairing the heart: what can we learn from embryonic development?*" Biomed Res Int 2014: 679168.

Gan, J., et al. (2015). "*Integrative Analysis of the Developing Postnatal Mouse Heart Transcriptome*." PloS one 10(7): e0133288.

Gerdes, J., et al. (1984). "*Cell cycle analysis of a cell proliferation-associated human nuclear antigen defined by the monoclonal antibody Ki-67*." J Immunol 133(4): 1710-1715.

Glotzer, M. (2001). "*Animal cell cytokinesis*." Annu Rev Cell Dev Biol 17: 351-386.

Goldthwaite Jr, C. A. (2007). "*Mending a broken heart: Stem cells and cardiac repair*." Stem Cell Information.

Goto, H., et al. (2003). "*Aurora-B regulates the cleavage furrow-specific vimentin phosphorylation in the cytokinetic process*." J Biol Chem 278(10): 8526-8530.

Harvey, R. P. and N. Rosenthal (1999). Heart Development. New York, Gulf Professional Publishing.

Hirschy, A., et al. (2006). "*Establishment of cardiac cytoarchitecture in the developing mouse heart*." Dev Biol 289(2): 430-441.

Ieda, M., et al. (2009). "*Cardiac fibroblasts regulate myocardial proliferation through beta1 integrin signaling*." Dev Cell 16(2): 233-244.

Ikenishi, A., et al. (2012). "*Cell cycle regulation in mouse heart during embryonic and postnatal stages*." Dev Growth Differ 54(8): 731-738.

Jain, R., et al. (2011). "*Cardiac neural crest orchestrates remodeling and functional maturation of mouse semilunar valves*." J Clin Invest 121(1): 422-430.

Kajstura, J., et al. (2010). "*Myocyte turnover in the aging human heart*." Circ Res 107(11): 1374-1386.

Kajstura, J., et al. (1998). "*Myocyte proliferation in end-stage cardiac failure in humans*." Proc Natl Acad Sci U S A 95(15): 8801-8805.

Kalluri, R. and R. A. Weinberg (2009). "*The basics of epithelial-mesenchymal transition*." J Clin Invest 119(6): 1420-1428.

Kaneko, H., M. Okamoto and K. Goshima (1984). "*Structural change of myofibrils during mitosis of newt embryonic myocardial cells in culture*." Exp Cell Res 153(2): 483-498.

Kirby, M. (1987). "*Cardiac Morphogenesis - Recent Research Advances*." Pediatr Res 21(3): 219-224.

Kosaka, Y., et al. (2012). "*14-3-3epsilon plays a role in cardiac ventricular compaction by regulating the cardiomyocyte cell cycle*." Mol Cell Biol 32(24): 5089-5102.

Kuhn, B., et al. (2007). "*Periostin induces proliferation of differentiated cardiomyocytes and promotes cardiac repair*." Nat Med 13(8): 962-969.

Kuriyama, S. and R. Mayor (2008). "*Molecular analysis of neural crest migration*." Philos Trans R Soc Lond B Biol Sci 363(1495): 1349-1362.

Laflamme, M. A., et al. (2007). "*Cardiomyocytes derived from human embryonic stem cells in pro-survival factors enhance function of infarcted rat hearts*." Nat Biotechnol 25(9): 1015-1024.

Laflamme, M. A. and C. E. Murry (2005). "*Regenerating the heart*." Nat Biotechnol 23(7): 845-856.

Laflamme, M. A. and C. E. Murry (2011). "*Heart regeneration*." Nature 473(7347): 326-335.

Laugwitz, K. L., et al. (2008). "*Islet1 cardiovascular progenitors: a single source for heart lineages?*" Development 135(2): 193-205.

Leu, M., E. Ehler and J. C. Perriard (2001). "*Characterisation of postnatal growth of the murine heart*." Anat Embryol (Berl) 204(3): 217-224.

Li, F., et al. (1997a). "*Formation of binucleated cardiac myocytes in rat heart: I. Role of actin-myosin contractile ring*." J Mol Cell Cardiol 29(6): 1541-1551.

Li, F., et al. (1996). "*Rapid transition of cardiac myocytes from hyperplasia to hypertrophy during postnatal development*." J Mol Cell Cardiol 28(8): 1737-1746.

Li, F., X. Wang and A. M. Gerdes (1997b). "*Formation of binucleated cardiac myocytes in rat heart: II. Cytoskeletal organisation*." J Mol Cell Cardiol 29(6): 1553-1565.

Lin, C. J., et al. (2012). "*Partitioning the heart: mechanisms of cardiac septation and valve development*." Development 139(18): 3277-3299.

Lyons, G. E. (1996). "*Vertebrate heart development*." Current Opinion in Genetics & Development 6(4): 454-460.

Mahmoud, A. I., et al. (2013). "*Meis1 regulates postnatal cardiomyocyte cell cycle arrest*." Nature 497(7448): 249-253.

Makkar, R. R., et al. (2012). "*Intracoronary cardiosphere-derived cells for heart regeneration after myocardial infarction (CADUCEUS): a prospective, randomised phase 1 trial*." Lancet 379(9819): 895-904.

Malliaras, K. and E. Marban (2011). "*Cardiac cell therapy: where we've been, where we are, and where we should be headed*." Br Med Bull 98(1): 161-185.

Manner, J., et al. (2001). "*The origin, formation and developmental significance of the epicardium: a review*." Cells Tissues Organs 169(2): 89-103.

Marín-García, J. (2011). Signaling in the Heart, Springer US.

Matsuura, K., et al. (2004). "*Adult cardiac Sca-1-positive cells differentiate into beating cardiomyocytes*." J Biol Chem 279(12): 11384-11391.

Matsuura, K., et al. (2012). "*Creation of human cardiac cell sheets using pluripotent stem cells*." Biochem Biophys Res Commun 425(2): 321-327.

Meilhac, S. M., et al. (2004). "*Oriented clonal cell growth in the developing mouse myocardium underlies cardiac morphogenesis*." J Cell Biol 164(1): 97-109.

Meilhac, S. M., et al. (2003). "*A retrospective clonal analysis of the myocardium reveals two phases of clonal growth in the developing mouse heart*." Development 130(16): 3877-3889.

Messina, E., et al. (2004). "*Isolation and expansion of adult cardiac stem cells from human and murine heart*." Circ Res 95(9): 911-921.

Mollova, M., et al. (2013). "*Cardiomyocyte proliferation contributes to heart growth in young humans*." Proc Natl Acad Sci U S A 110(4): 1446-1451.

Moorman, A. F. and V. M. Christoffels (2003). "*Cardiac chamber formation: development, genes, and evolution*." Physiol Rev 83(4): 1223-1267.

Nag, A. C. (1980). "*Study of non-muscle cells of the adult mammalian heart: a fine structural analysis and distribution*." Cytobios 28(109): 41-61.

Naqvi, N., et al. (2014). "*A proliferative burst during preadolescence establishes the final cardiomyocyte number*." Cell 157(4): 795-807.

Ng, W. A., et al. (1991). "*Cardiac myosin heavy chain mRNA expression and myocardial function in the mouse heart*." Circ Res 68(6): 1742-1750.

Olivetti, G., et al. (1996). "*Aging, cardiac hypertrophy and ischemic cardiomyopathy do not affect the proportion of mononucleated and multinucleated myocytes in the human heart*." J Mol Cell Cardiol 28(7): 1463-1477.

Oparil, S. (1985). "*Pathogenesis of ventricular hypertrophy*." J Am Coll Cardiol 5(6 Suppl): 57B-65B.

Oparil, S., S. P. Bishop and F. J. Clubb, Jr. (1984). "*Myocardial cell hypertrophy or hyperplasia*." Hypertension 6(6 Pt 2): III38-43.

Orkin, S. H. and L. I. Zon (2008). "*Hematopoiesis: an evolving paradigm for stem cell biology*." Cell 132(4): 631-644.

Oyama, K., et al. (2014). "*Epigenetic regulation of cardiac myocyte differentiation*." Front Genet 5: 375.

Park, D. S., et al. (2013). "*Pocket proteins critically regulate cell cycle exit of the trabecular myocardium and the ventricular conduction system*." Biol Open 2(9): 968-978.

Pasumarthi, K. B. and L. J. Field (2002). "*Cardiomyocyte cell cycle regulation*." Circ Res 90(10): 1044-1054.

Perriard, J. C., A. Hirschy and E. Ehler (2003). "*Dilated cardiomyopathy: a disease of the intercalated disc?*" Trends Cardiovasc Med 13(1): 30-38.

Pfister, O., et al. (2005). "*CD31- but Not CD31+ cardiac side population cells exhibit functional cardiomyogenic differentiation*." Circ Res 97(1): 52-61.

Porrello, E. R., et al. (2011). "*Transient regenerative potential of the neonatal mouse heart*." Science 331(6020): 1078-1080.

Puente, B. N., et al. (2014). "*The oxygen-rich postnatal environment induces cardiomyocyte cell-cycle arrest through DNA damage response*." Cell 157(3): 565-579.

Raulf, A., et al. (2015). "*Transgenic systems for unequivocal identification of cardiac myocyte nuclei and analysis of cardiomyocyte cell cycle status*." Basic Res Cardiol 110(3): 489.

Risebro, C. A. and P. R. Riley (2006). "*Formation of the ventricles*." ScientificWorldJournal 6: 1862-1880.

Sarantitis, I., et al. (2012). "*The cytoskeleton of the cardiac muscle cell*." Hellenic J Cardiol 53(5): 367-379.

Sdek, P., et al. (2011). "*Rb and p130 control cell cycle gene silencing to maintain the postmitotic phenotype in cardiac myocytes*." J Cell Biol 194(3): 407-423.

Sedmera, D., et al. (2000). "*Developmental patterning of the myocardium*." Anat Rec 258(4): 319-337.

Senyo, S. E., et al. (2013). "*Mammalian heart renewal by pre-existing cardiomyocytes*." Nature 493(7432): 433-436.

Soonpaa, M. H. and L. J. Field (1997). Assessment of cardiomyocyte DNA synthesis in normal and injured adult mouse hearts.

Soonpaa, M. H., et al. (1996). "*Cardiomyocyte DNA synthesis and binucleation during murine development*." Am J Physiol 271(5 Pt 2): H2183-2189.

Steinhauser, M. L. and R. T. Lee (2011). "*Regeneration of the heart*." EMBO Mol Med 3(12): 701-712.

Studzinski, G. P. and L. E. Harrison (1999). "*Differentiation-related changes in the cell cycle traverse*." Int Rev Cytol 189: 1-58.

Takehara, N., et al. (2008). "*Controlled delivery of basic fibroblast growth factor promotes human cardiosphere-derived cell engraftment to enhance cardiac repair for chronic myocardial infarction*." J Am Coll Cardiol 52(23): 1858-1865.

Tam, P. P., et al. (1997). "*The allocation of epiblast cells to the embryonic heart and other mesodermal lineages: the role of ingression and tissue movement during gastrulation*." Development 124(9): 1631-1642.

Tane, S., et al. (2014a). "*CDK inhibitors, p21(Cip1) and p27(Kip1), participate in cell cycle exit of mammalian cardiomyocytes*." Biochem Biophys Res Commun 443(3): 1105-1109.

Tane, S., et al. (2014b). "*Repression of cyclin D1 expression is necessary for the maintenance of cell cycle exit in adult mammalian cardiomyocytes*." J Biol Chem 289(26): 18033-18044.

Tzahor, E. and S. M. Evans (2011). "*Pharyngeal mesoderm development during embryogenesis: implications for both heart and head myogenesis*." Cardiovasc Res 91(2): 196-202.

Vincent, S. D. and M. E. Buckingham (2010). "*How to make a heart: the origin and regulation of cardiac progenitor cells*." Curr Top Dev Biol 90: 1-41.

Vliegen, H. W., et al. (1991). "*Myocardial changes in pressure overload-induced left ventricular hypertrophy. A study on tissue composition, polyploidization and multinucleation*." Eur Heart J 12(4): 488-494.

Walsh, R. A. (2005). Molecular Mechanisms of Cardiac Hypertrophy and Failure. United Kingdom, CRC Press.

Walsh, S., et al. (2010). "*Cardiomyocyte cell cycle control and growth estimation in vivo--an analysis based on cardiomyocyte nuclei*." Cardiovasc Res 86(3): 365-373.

Webb, S., N. A. Brown and R. H. Anderson (1998). "*Formation of the atrioventricular septal structures in the normal mouse*." Circ Res 82(6): 645-656.

Wessels, A. and D. Sedmera (2003). "*Developmental anatomy of the heart: a tale of mice and man*." Physiol Genomics 15(3): 165-176.

WHO (2010). Global status report on noncommunicable diseases 2010. Geneva, World Health Organization (WHO).

WHO (2011). Global atlas on cardiovascular disease prevention and control. Geneva, World Health Organization (WHO).

Wills, A. A., et al. (2008). "*Regulated addition of new myocardial and epicardial cells fosters homeostatic cardiac growth and maintenance in adult zebrafish*." Development 135(1): 183-192.

Xin, M., E. N. Olson and R. Bassel-Duby (2013). "*Mending broken hearts: cardiac development as a basis for adult heart regeneration and repair*." Nat Rev Mol Cell Biol 14(8): 529-541.

Zhang, W., et al. (2013). "*Molecular mechanism of ventricular trabeculation/compaction and the pathogenesis of the left ventricular noncompaction cardiomyopathy (LVNC)*." Am J Med Genet C Semin Med Genet 163C(3): 144-156.

WEBSITES

1. "National Heart, Lung and Blood Institute (USA.gov) - What Is a Ventricular Assist Device?", cited 13-10-2014, from http://www.nhlbi.nih.gov/health/health-topics/topics/vad/#.

SUPPLEMENTAL MATERIAL

Supplementary Table 1: Statistic data source.

	n value			
Fig.9	E10.5	10 / 80	*# Replicates* / *Hearts*	
	E13.5	9 / 72		
	E17.5	15 / 15		
	P0	7 / 7		
	P3	6 6		
	P10	2 / 2		
	P15	1 / 1		
	P24	1 / 1		
	Adult (NP;P)*	6/6;1/1		
Fig.10	E10.5	26463	*# CMs*	
	E13.5	44513		
	E17.5	49036		
	P0	36379		
	P3	24157		
	P10	5613		
Fig.12	E10.5	414	*# CMs*	
	E13.5	281		
	E17.5	319		
	P0	156		
	P3	386		
	P10	94		
Fig.14		*# Hearts*	*Ki67* *#Cells* / *Nuclei+* / *CMs+*	*pH3* *#Cells* / *Nuclei+* / *CMs+*
	E10.5	4	69853 / 538 / 324	28984 / 433 / 226
	E13.5	4	184783 / 4036 / 3006	90225 / 1233 / 658
	E17.5	4	248934 / 5684 / 4533	30675 / 2331 / 1452
	P0	4	320903 / 9773 / 7971	470018 / 5176 / 2789
	P3	4	563353 / 8138 / 5660	750793 / 2254 / 1109
	P7	4	527354 / 2609 / 1769	672691 / 1347 / 614
	P10	4	559128 / 1142 / 566	1033975 / 1144 / 558
	P15	4	964373 / 1930 / 1040	1725787 / 594 / 194
	P24	2	531547 / 238 / 113	228614 / 50 / 17
	Adult	4	1027624 / 833 / 273	1444320 / 439 / 120
Fig.15	E10.5	6889 / 1279	*# total cells* / *CMs*	
	E13.5	3907 / 1432		
	E17.5	2371 / 1103		

*NP: non-perfused hearts; P: 4% PFA-perfused hearts.